Report from:

(2)

THE SOLID STATE CHEMISTRY GROUP AT UMIST

Chemistry Department
UMIST
Sackville Street
Manchester M60 1QD
U.K.

UNCLASSIFIED
SECURITY CLASSIFICATION OF THIS PAGE

REPORT DOCUMENTATION PAGE

1a. REPORT SECURITY CLASSIFICATION UNCLASSIFIED	1b. RESTRICTIVE MARKINGS
2a. SECURITY CLASSIFICATION AUTHORITY	3 DISTRIBUTION / AVAILABILITY OF REPORT
2b DECLASSIFICATION / DOWNGRADING SCHEDULE	
4. PERFORMING ORGANIZATION REPORT NUMBER(S)	5. MONITORING ORGANIZATION REPORT NUMBER(S) EOARD-TR-89-89
6a. NAME OF PERFORMING ORGANIZATION University of Manchester Industrial Sci & Tech (UMIST) 6b. OFFICE SYMBOL (If applicable)	7a. NAME OF MONITORING ORGANIZATION European Office Aerospace Research & Development (EOARD)
6c. ADDRESS (City, State, and ZIP Code) Dept of Chemistry & Centre for Electronic P.O. Box 88 Manchester M60 1QD United Kingdom	7b. ADDRESS (City, State, and ZIP Code) Box 14 FPO New York 09510
8a. NAME OF FUNDING / SPONSORING ORGANIZATION European Office of Aerospace Research & Development 8b OFFICE SYMBOL (If applicable) LRE	9 PROCUREMENT INSTRUMENT IDENTIFICATION NUMBER
8c. ADDRESS (City, State, and ZIP Code) Box 14 FPO New York 09510	10 SOURCE OF FUNDING NUMBERS PROGRAM ELEMENT NO. 61102F; PROJECT NO. 2301; TASK NO. D1; WORK UNIT ACCESSION NO 001

11 TITLE (Include Security Classification)

ZINC TELLURIDE GROWTH ON InP

12 PERSONAL AUTHOR(S)

PROFESSOR J O WILLIAMS AND DR NICHOLAS MAUNG

13a. TYPE OF REPORT	13b. TIME COVERED	14. DATE OF REPORT (Year, Month, Day)	15. PAGE COUNT
ANNUAL	FROM TO	1989	

16 SUPPLEMENTARY NOTATION

17 COSATI CODES			18. SUBJECT TERMS (Continue on reverse if necessary and identify by block number)
FIELD	GROUP	SUB-GROUP	
			ZnTe; MOCVD

19. ABSTRACT (Continue on reverse if necessary and identify by block number)

Initial studies have concentrated on the preparation of epitaxial ZnSe on InP(100) substrates and an optimum bakeout procedure for the substrates determined. Subsequently, the doping of ZnSe with small amounts of Te (up to ca 5 at %) was achieved and the structural, compositional and optical properties of the epitaxial layers investigated. It was demonstrated by photoluminescence measurement that in small concentrations (~2 at %) Te acts as an isolated isoelectronic trap in ZnSe and at higher concentrations clusters of Te atoms form. This results in broadened photoluminescence emission peaks. It proved impossible with our atmospheric pressure MOCVD reactor and using a conventional source of Te to prepared epitaxial layers of the ternary $ZnSe_{1-y}Te_y$ with Te concnetration in excess of ca 5 at %.

20. DISTRIBUTION / AVAILABILITY OF ABSTRACT XX UNCLASSIFIED/UNLIMITED ☒ SAME AS RPT ☐ DTIC USERS	21. ABSTRACT SECURITY CLASSIFICATION UNCLASSIFIED
22a. NAME OF RESPONSIBLE INDIVIDUAL D. Eirug Davies, PhD	22b. TELEPHONE (Include Area Code) 44 (0)1-409-4318 22c. OFFICE SYMBOL EOARD/LRE

DD FORM 1473, 84 MAR 83 APR edition may be used until exhausted. All other editions are obsolete.

SECURITY CLASSIFICATION OF THIS PAGE
UNCLASSIFIED

EOARD-TR-89-09

This report has been reviewed and is releasable to the National Technical Information Service (NTIS). At NTIS it will be releasable to the general public, including foreign nations.

This technical report has been reviewed and is approved for publication.

EIRUG DAVIES, Ph.D.
Chief, Semiconductor/S.S. Phys

FRED T. GILLIAM, Lt Col, USAF
Chief Scientist

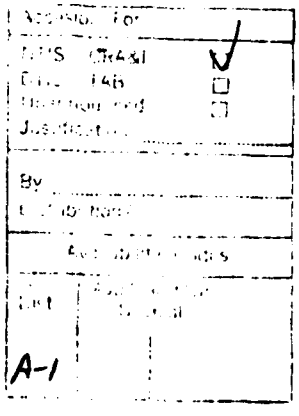

UMIST GRANT AFOSR-88-0109

FINAL REPORT ON THE GROWTH AND CHARACTERISATION OF $ZnSe_{1-x}Te_x$ LAYERS ON GaAs(100) and InP(100) BY METAL ORGANIC VAPOUR PHASE EPITAXY (MOVPE)

N. Maung
J.O. Williams
14 January 1989

AFOSR-88-0109

Zinc Selenide Telluride Growth on InP

OBJECTIVE

The main objective of this one year programme was to investigate MOCVD as a preparative technique for $ZnSe_{1-y}Te_y$ thin films with Te concentration suitable for lattice matching of epitaxial layers to InP substrates ie (Te) = 0.46. A secondary aim was to add impurities to the layers in order to reproducibly achieve p- and n-type

SUMMARY OF PROGRESS

Initial studies have concentrated on the preparation of epitaxial ZnSe on InP(100) substrates and an optimum bakeout procedure for the substrates determined. Subsequently, the doping of ZnSe with small amounts of Te (up to ca 5 at %) was achieved and the structural, compositional and optical properties of the epitaxial layers investigated. It was demonstrated by photoluminescence measurement that in small concentrations ($\sim$2 at %) Te acts as an isolated isoelectronic trap in ZnSe and at higher concentrations clusters of Te atoms form. This results in broadened photoluminescence emission peaks. It proved impossible with our atmospheric pressure MOCVD reactor and using a conventional source of Te to prepare epitaxial layers of the ternary $ZnSe_{1-y}Te_y$ with Te concentration in excess of ca 5 at %.

INTRODUCTION

Since the original intention of the present work was to grow lattice matched $ZnSe_{0.56}Te_{0.44}$/InP(100), growth of ZnSe on InP(100) was attempted initially in order to evaluate the efficiency of the substrate bake-out procedure. Subsequent to this, growth of ZnSe doped with very small amounts of tellurium (hereafter referred to as ZnSe:Te) was attempted to establish both cracking efficiency of the tellurium precursor used and the subsequent behaviour of tellurium in the host lattice. The ZnSe/GaAs(100) system was chosen specifically for this purpose since it is one with which we are very familiar and have conducted extensive investigations.

Following on from this, growth of $ZnSe_{1-x}Te_x$ on InP(100) was attempted and subsequent characterisation was carried out, using optical microscopy, double crystal X-ray diffraction and photoluminescence spectroscopy. Energy dispersive analysis of X-rays, EDAX, was used to evaluate the tellurium content of the deposited layers.

EXPERIMENTAL DETAILS

All the epitaxial films discussed in this report were grown by atmospheric pressure metal organic vapour phase epitaxy (MOVPE) using a system described previously[1].. Diethylzinc (Epichem), H_2Se (5% in hydrogen : BOC Special Gases) and Diispropyltelluride (DIPT - St Andrews University) were used as the source materials and the growth conditions relevant to each series of experiments are given in the appropriate sections.

The sample thickness and surface morphology was examined by optical microscopy (Olympus microscope). Double crystal X-ray diffraction measurements were performed using a Bede Scientific Instruments QCI diffractometer. An InP substrate was used as the first crystal and in all cases the surface symmetric 400 reflection ws used in the (+−) parallel arrangement, non dispersive in wavelength.

Analysis of the double crystal rocking curves provides directly the lattice mismatch and a measure of layer and substrate perfection.

Photolumminescence (PL) measurements were performed using a system described previously[1] at temperatures varying from room temperature down to ? K. The spectral resolution in the region of interest is better than 1.0 cm^{-1}.

Energy dispersive analysis of X-rays (EDAX) was used to evaluate the extent of tellurium incorporation in all $ZnSe_{1-x}Te$ and ZnSe:Te layers using a Philips 505 scanning electron microscope SEM.

1. Growth and Characterisation of ZnSe on InP(100) and InAs(100) substrates. A Comparison with ZnSe/GaAs(100) of the Effects of Lattice Mismatch and Substrate Bakeout Procedure.

The intention of growing ZnSe epilayers on InP(100) and InAs(100) substrates was to try to evaluate the effects of the substrate preparation and bakeout procedure on the film properties. InP and InAs were chosen as the substrate materials since growth of $ZnSe_{0.54}Te_{0.46}$ lattice matched to InP was the main aim of the project, whilst $ZnSe_{0.10}Te_{0.90}$ lattice matched to InAs lies at the tellurium rich end of the ZnSe-ZnTe tie line and preliminary experiments concerning ZnTe growth on InAs(100) would probably be carried out later. Comparison with ZnSe grown on GaAs(100), for which the film properties are well known, would then allow jundgements to be made concerning the effectiveness of the bakeout procedure.

A study of the bakeout procedure is required since on the present MOVPE growth system there is no provision for either arsine (AsH_3) or phosphine (PH_3) sources. Normally, in III-V semiconductor growth of materials on InP or InAs substrates, a pre-growth bakeout at elevated temperatures (> 700°C) with either PH_3/H_2 for growth on InP or AsH_3/H_2 for growth on InAs is carried out[2]. This treatment is believed to clean the growth surface, remove the surface oxide and importantly reduce the amount of the volatile group V element lost through evaporation at high bakeout temperatures. In the present case, subsequent to the wet chemical preparation stage[2] only a bakeout under hydrogen at relatively low temperatures could be performed.

This was necessary in order to avoid excess loss of the group V component and a subsequently non-stoichiometric seed surface on which growth would commence. Obviously, the effects of such treatment on film properties need to be evaluated if growth of multi component systems on these substrates is to be contemplated.

RESULTS & DISCUSSIONS

Growth

ZnSe epilayers were grown on both InP(100) and InAs(100) substrates using established chemical cleaning procedures, bakeout programs and growth conditions listed the Table 1. The growth rates obtained were 17 μmhr^{-1} for ZnSe/InP(100) and 12 μmhr^{-1} for ZnSe/InAs(100). Under the same conditions ZnSe grows at 20 μmhr^{-1} on GaAs(100). Resulting layers were generally 4-14 μm thick.

Total hydrogen flow rate (cm^3/min)	1600
Hydrogen flow rate through DMZ bubbler (cm^3/min)	16.7
Temperature of DMZ bubbler (°C)	-18°C
Flow rate of 5 % H_2Se/H_2 (Cm^3/min)	32.9
VI/II ratio	1:5
Growth temperature (°C)	280

Sample no.	ZnSe/Substrate system	Bakeout time (mins)	Bakeout temp (°C)
NM 1	ZnSe/InP(100)	20	600
NM 2	ZnSe/InP(100)	60	400
NM 3	ZnSe/InP(100)	30	500
NM 4	ZnSe/InAs(100)	10	500
NM 5	ZnSe/InAs(100)	30	500

TABLE 1

Typical Growth Conditions for ZnSe on InP(100) and InAs(100).

Optical Microscopy

The surfaces of the heteroepitaxial films obtained on all substrates, including GaAs(100) appeared extremely smooth and relatively shiny to the naked eye. In this comparison, ZnSe grown on GaAs(100) produced the best surfaces and in some cases was almost specular!

Dark field and phase contrast microscopies, however, revealed pyramidal features, crosshatches and terraces although these features did not appear to depend on the substrate bakeout procedures. Fig 1 shows a representative optical photo micrograph of an 8.5 μm thick ZnSe layer grown on InP(100) baked out at 500°C for 30 mins, NM3. Once again, ZnSe grown on GaAs(100) showed the most featureless surfaces especially for layers thicker than 5 μm. Uniformity of growth as evidenced from cleaved (110) sections, was good in all cases, but with some slight cracking in the ZnSe layers grown on InP(100) and InAs(100) substrates.

Cracking, crosshatches and terraces have all been attributed to the presence of misfit dislocations occurring at the interface of lattice mismatched heteroepitaxial systems. In this context growth of ZnSe on GaAs ($\Delta a/a$ = +0.27%) would be expected to be superior to growth of ZnSe on InP ($\Delta a/a$ = -3.41%) and growth of ZnSe on InAs ($\Delta a/a$ = -6.43%). These features appear, however, to have little effect on the layer crystallographic properties, discribed in the next section.

Double Crystal X-ray Diffraction Analysis

Since an InP first crystal was used but GaAs and InAs as well as InP substrates were used for ZnSe growth the rocking curve broadens by an amount $\Delta\theta^1$ over the intrinsic linewidth due to the differing lattice parameters of the specimen (both the ZnSe epilayers and substrate material have to be considered separately) and reference crystals[3].

The reason for this is that the intersection point of the range of angles over which Bragg reflection will occur as a function of wavelength for the reference and specimen crystals is extremely narrow and moves rather slowly with the angle of misorientation.

The values of $\Delta\theta_\lambda^1$ pertaining to 400 CuKα radiation for the materials used here are shown in Table 2.

Specimen crystal	$\Delta\theta_\lambda^1$ /arc secs
InP	0
GaAs	17
InAs	13
ZnSe	16

TABLE 2

Amount by which intrinsic rocking curves are broadened, $\Delta\theta_\lambda^1$, using an InP reference crystal set up for the 400 reflection and CuK radiation.

As can be seen from Fig 2, baking out of the InP substrate at different temperatures has little effect on the crystallographic properties of the resulting ZnSe layers. Similar behaviour was observed for ZnSe layers grown on InAs baked out at various substrate temperatures, not shown.

As Tables 3 and 4 show for ZnSe layers grown on InP at 280°C, lower bakeout temperatures appear to lead to better crystallographic properties, viz smaller layer FWHM values and reduced magnitudes of lattice mismatch. Indeed the structural properties of ZnSe layers grown on InP appear to be superior to those grown on InAs and surprisingly GaAs substrates, see Fig 3a,b, in spite of the much larger lattice mismatch between ZnSe/InP ($\Delta a/a$ = -6.43%) compared to ZnSe/GaAs ($\Delta a/a$ = +0.27%). This result is repeatable and the values listed in Tables 3 and 4 are averages taken from three indentical sets of samples. It is known, however, that structural properties do depend on layer thickness and so the results reported may not show definitive variations of $\Delta\theta$, with different substrate materials

The FWHM values of the layer and substrate peaks represent a superposition of a number of independent Gaussian components. Superimposed upon the

intrinsic linewidths of the first and the second (sample) crystals are further extensive contributions, as well as $\Delta\theta_\lambda^1$. Contributions arise from lattice tilting, local strain, particle size and uniform lattice bending or curvature[4]. The effect of increasing strain and varying particle size is to broaden the rocking curve. Conversely sample curvature reduces the FWHM of the epilayer peak. However, it is more likely in the present case that the linewidth is dominated by lattice tilting and accompanying dislocations, ie, single crystal grains of the epilayer are tilted slightly out of the substrate plane. This would manifest itself in a variation of lattice mismatch under different growth conditions as well as an increase in epilayer FWHM. Additionally, thermal strains induced by the difference in thermal expansion coefficients between the epilayer and substrate may contribute to the observed variations in the FWHM with varying bakeout temperatures for the different substrate materials. In this connection one would expect a reduction in the amount of thermal expansion mismatch from ZnSe/InP through ZnSe/InAs to ZnSe/GaAs.

Photoluminescence Properties

The PL spectrum of one of the ZnSe epilayers grown on InP is shown in Fig 4a. This specimen was baked out at 400°C and is 8.5 μm thick. The emission spectrum of this sample is representative of the spectra obtained for all samples in this study. The spectrum is dominated by I_X, the intense peak centred near 2.7941 eV due to recombination of excitons bound to neutral donors. The intensity of the deep-level (DL) emission, taken to be luminescence with energy less than 2.4 eV, was found to be typically one order of magnitude smaller than the intensity of the near band edge, (NBE) emission due to I_X. The ratio of the intensities of the NBE emission to the DL emission is referred to as the R value and is taken to be a measure of sample quality. The linewidth and intensity of the dominant NBE emission, ΔE and I_T, respectively, are also used to assess the relative quality of the epilayers. High quality epilayers exhibit small ΔE values, large R values and large I_T values.

As can be seen from Table 5, ZnSe films grown on GaAs have superior luminescence properties to those grown on InP and InAs substrates. Representative spectra of ZnSe epilayers deposited on InAs and GaAs

Sample No.	ZnSe/substrate system	Bakeout temperature (°C)	Layer thickness 1 μm	FWHM ZnSe $\Delta\theta$/arc sec uncorrected	FWHM Substrate $\Delta\theta$/arc sec uncorrected	$\Delta\theta_1/\Delta\theta_2$	Mismatch /ppm
NM 1	ZnSe/InP(100)	600	8.5	164	43	3.81	$-4.0242 \times 10^{-}$
NM 2	ZnSe/InP(100)	400	8.5	134	45	2.98	$-3.4662 \times 10^{-}$
NM 3	ZnSe/InP(100)	500	8.5	185	40	4.63	$-3.9991 \times 10^{-}$
NM 4	ZnSe/InAs(100)	500	6	228	50	4.56	$-6.4616 \times 10^{-}$
NM 5	ZnSe/InAs(100)	500	6	257	53	4.84	$-6.4542 \times 10^{-}$
NM 6	ZnSe/InP(100)	600	13	150	43	3.49	$-3.8262 \times 10^{-}$
NM 99	ZnSe/GaAs(100)	550	5.25	213	49	4.35	$+2.2077 \times 10^{-}$
NM 105	ZnSe/GaAs(100)	550	2	320	45	7.11	$+2.6851 \times 10^{-}$

TABLE 3

Dependence of ZnSe film structural properties
on substrate bakeout temperatures.
All films were grown at 280 °C under identical conditions
except NM 105, grown at 400 °C.

Sample no	ZnSe/substrate system	FWHM ZnSe $\Delta\theta_1^u$/arc sec uncorrected	FWHM ZnSe $\Delta\theta_1^c$/arc sec corrected	FWHM substrate $\Delta\theta_2^u$/arc sec uncorrected	FWHM substrate $\Delta\theta_2^c$/arc sec corrected	$\Delta\theta_1^u / \Delta\theta_2^u$	$\Delta\theta_1^c / \Delta\theta_2^c$
NM 1	ZnSe/InP(100)	164	148	43	43	3.81	3.44
NM 2	ZnSe/InP(100)	134	118	45	45	2.98	2.62
NM 3	ZnSe/InP(100)	185	169	40	40	4.63	4.23
NM 4	ZnSe/InAs(100)	228	212	50	37	4.56	5.73
NM 5	ZnSe/InAs(100)	257	241	53	40	4.85	6.03
NM 6	ZnSe(InP(100)	150	134	43	43	3.49	3.12
NM 99	ZnSe/GaAs(100)	213	197	49	32	4.35	6.16
NM 105*	ZnSe/GaAs(100)	320	304	45	28	7.11	10.90

TABLE 4

Corrected Values of Structural parameters allowing for δ_λ broadening effects.
All films were grown at 280 °C under identical conditions except NM 105
grown at 400 °C.

Sample no.	ZnSe/substrate system	Bakeout temperature (°C)	Layer Thickness /μm	Δ E/meV	R	I_T/arb units
NM 1	ZnSe/InP(100)	600	8.5	15.7	1[illegible]	2.7×10^4
NM 2	ZnSe/InP(100)	400	8.5	6.6	30.5	3.06×10^5
NM 3	ZnSe/InP(100)	500	8.5	14.9	13.5	5.1×10^4
NM 4	ZnSe/InAs(100)	500	6	6.2	40	4.5×10^5
NM 5	ZnSe/InAs(100)	500	6	13.1	11.2	3.8×10^5
NM 6	ZnSe/InP(100)	600	13	21.8	5	3.0×10^4
NM 99	ZnSe/GaAs(100)	550	5.25	3.2	3.5×10^3	3.1×10^6
NM 105	ZnSe/GaAs(100)	550	2	2	50	4.2×10^4

KEY: Δ E - width of the dominant NBE peak, generally I_x. R - ratio of the dominant NBE peak, to the dominant DL peak intensities. I_T - intensity of the dominant NBE emission.

TABLE 5

Dependence of the low temperature PL (10 K) properties on the bakeout temperatures of the various substrate materials

However, room temperature PL emission can still be obtained for ZnSe layers grown on InP, NM2, as Fig 4d shows. The room temperature NBE emission appears at 2.687 ev (ΔE = 53.2 meV) albeit with low PL efficiency (R = 3.2). For comparison ZnSe grown on GaAs, NM99 has a room temperature NBE emission of 2.696 eV(ΔE = 44meV) and a PL efficiency (R = 35) higher by an order of magnitude. (Theoretically, one would expect the band to band emission to occur at 2.693 eV with a ΔE of 3/2 kT (eg 38 meV).

The apparent inconsistency between the PL and X-ray results can be rationalised if one remembers that the better crystallinigy of the ZnSe layers grown on InP compared to those grown on GaAs is modulated in the luminescence properties by an inferior surface morphology.

A poor surface morphology migh be expected to induce a broad continuum of non-radiative and trapping surface states. These would attenuate the values of I_T and R by reducing the exciton lifetime. That is efficient migration of excitons to non-radiative surface states before recombination would reduce the efficiency of both the I_T emission and the value of R, especially under the low excitation conditions used here. such a mechanism would also have the effect of increasing ΔE directly, as is observed.

CONCLUSION

It appears that a bakeout temperature of 500°C is suitable for ZnSe growth on InAs(100) but a bakeout temperature of 400°C to500°C is probably more appropriate for ZnSe growth on InP(100) under growth conditions which lead to optimal material properties in the ZnSe/GaAs(100) system.

However, the optical quality of such material is significantly inferior to standard ZnSe grown on GaAs, primarily due to a poor surface morphology.

2. Growth and Characterisation of ZnSe:Te on GaAs(100)

INTRODUCTION

Tellurium can act both as an isoelectronic trap and as a constituent of the corresponding alloy, $ZnSe_{1-x}Te_x$ depending upon its concentration in the host lattice of ZnSe[5]. In the dilute limit an isoelectronic atom in a binary compound, the case here for ZnSe:Te, can be regarded as an impurity while at high concentrations it can be regarded as a constituent of the alloy, $ZnSe_{1-x}Te_x$.

Isoelectronic impurities incorporated into binary compounds introduce trapping potentials due to differences in electronegativity. If the impurity is less electronegative than the host atom it replaces (eg Te in ZnSe), a hole is localised by the strong short range interaction. Subsequently, an electron is bound by Coulombic interaction to form a strongly localised exciton at the isoelectronic trap.

Two forms of behaviour have been identified for Te in various II-VI compounds. In Cd $S_{1-x}Se_x$ doped with Te[6] when the impurity concentration is small, sharp emission bands due to localised excitons are observed; as the impurity concentration is increased, the spectra show both a gradual shift in peak energy and a broadening of the exciton line width due to statistical fluctuations in the random alloy potential. That is in this case Te behaves as a constituent of a random alloy. The optical properties varying smoothly with band gap as a function of Te concentration for $CdS_{1-x}Te_x$ on the other hand, strong localisation of excitons occurs at clusters containing one or more Te atoms together with large lattice relaxation at Te lattice sites; when the Te concentration is small, the bound excitons localise at single Te sites, while at higher concentrations localisation of the exciton occurs at Te clusters, which have much larger binding energies. That is in this case the emission bands shift somewhat irregularly with increasing Te concentration, depending upon the dominant form of Te cluster size (Te_n (n = 1,2,3,4.)), to lower energy.

Little work has so far been done on the $ZnSe_{1-x}Te_x$ system[5,8,9], and none to date by MOVPE. The purpose of this study is to report on very low levels of Te impurities in ZnSe using a novel Te precursor, diisopropyl telluride,

hereafter referred to as DIPT. This reagent has been used to replace the more usual Te source, diethyltelluride. It has higher vapour pressure and would be expected to yield higher Te concentrations in the epitaxial material.

RESULTS & DISCUSSIONS

Growth

ZnSe epilayers doped with Te were grown on GaAs(100) substrates (n-type) using the growth conditions listed the Table 6. The growth rates obtained were 18.8 μm hr^{-1} at 280°C, 16.9 μm hr^{-1} at 330°C and 11.3 μm hr^{-1} at 370°C. Resulting layers were generally 2-6μm thick.

Total hydrogen flow rate (cm^3/min)	1600
Hydrogen flow rate through DMZ bubble (cm^3/min)	16.7
Temperature of DMZ bubbler (°C)	-18
Hydrogen flow rate through DIPT bubbler (cm^3/min)	14
Temperature of DIPT bubbler (°C)	27
Flow rate of 5% H_2Se/H_2 (cm^3/min)	80.7
VI/II ratio	4
Growth temperature, Tg, (°C)	280-370

TABLE 6

Growth Conditions for ZnSe:Te on GaAs(100)

The DIPT source (Professor D J Cole-Hamilton, Chemistry Department, University of St Andrews) has a boiling point of 157-159°C at atmospheric pressure. The partial pressure of DIPT in the reactor was calculated using

$$\log_{10}P\ (mmHg) = 7.07 - 1802/T(K)$$

A buffer layer of ZnSe was grown for 10 mins at each growth temperature prior to introduction of the DIPT. Only thin films of Te doped material could be produced (< 2 μm) owing to problems with exhaust effluent disposal in the present system.

Optical Scanning Electron Microscopy

All the specimens except those grown at 280°C exhibited rough surfaces, the degree of roughness increasing with increasing growth temperature and Te content. Fig 5 shows the surface morphology of a typical sample grown at 370°C. The surface is rough and exhibits a wavy like texture. By comparison, specimens grown at 280°C were smoother like normal, undoped ZnSe epilayers grown on GaAs(100). Specimens grown at 330°C fell in between these two extremes.

SEM photomicrographs for sample NM8 (Tg = 280°C) 4.9 μm thick are shown in Figs 6(a) and 6(b). The cross section in Fig 12(a) shows a fairly defective layer with cracks running through the entire ZnSe:Te layer from the GaAs substrate through to the ZnSe:Te free surface. Small black spots are visible throughout the layer and these may be due to a fine microstructure or possibly Te clusters. As Fig 6b) shows, these black spots are also visible on the layer surface, their local concentration varying over the sample surface.

Double Crystal X-ray Diffraction and EDAX Analysis

The concentration of Te in the grown crystals was measured by X-ray microanalysis. Since the detectivity in the EDAX analysis is approximately 0.1 at % it can be seen on examining Table 7 that all the grown layers have less than 0.5 at % of Te. This would appear to indicate that under the growth conditions employed, DIPT is not cracking efficiently to yield elemental Te. That is, in the present system a Tg of >370°C is necessary in order to obtain complete pyrolysis of DIPT. Indeed only by 450°C does decomposition appear to be complete.

Sample no. (Layer thickness)	Tg/(°C)	at % Te	FWHM ZnSe /arc sec	FWHM GaAs /arc sec	Mismatch/ ppm
NM8 (4.9 μm)	280	0.18	282	36	4.3259 x 10^{-3}
NM9 (4.5 μm)	330	0.21	241	46	3.3550 x 10^{-3}
NM10 (3 μm)	370	0.44	168	55	1.6408 x 10^{-3}

TABLE 7

Structural and Compositional Data for ZnSe:Te/GaAs(100)

Crystallinity of the resulting ZnSe:Te layers appears to be dominated by the dependence on Tg, see Figs 7 a-c. Over a range of 90°C the Te content of the layers increases by only 0.26 at % and would, therefore, not be expected to contribute significantly to the ZnSe linewidth. The trend is as expected for undoped ZnSe grown on GaAs(100). The reduction in lattice mismatch by almost a factor of 3 cannot be due to the incorporation of Te, since the opposite trend would be predicted on the basis of simple site replacement of Te for Se

Photoluminescence Properties

The low temperature (10 K) PL spectra of the Te doped layers exhibit strong new emission bands not observed in the spectra of the undoped ZnSe layers. A discussion of the three samples listed in Table 7 follows, but a detailed explanation of the optical processes involved is deferred until Section 3.

The PL spectrum of sample NM8(0.18 at % Te) is dominated by the neutral donor bound exciton line I_x, at 2.7953 eV, Fig 8a. This is the dominant emission line in nominally undoped ZnSe, see Section 1. However, at lower energy a broad undulating peak centred at 2.655 eV appears with a zero phonon line at 2.758 eV. This emission is absent in the nominally undoped

Sample no. Layer Thickness	at % Te ± 0.1%	Te emission peak E^{Te} (eV)	Stokes shift (meV) $\Delta_S = E^{ZnSe} - E^{Te}$	Huang-Rhys factors, S	Zero-phono energy E_o (eV)	Exciton binding energy $E^{Te} = E^{ZnSe} - E_o$ (meV)
NM 8 (4.9 μm)	0.18	2.655	147	1.8	2.758	44 ± 5
NM 9 (4.5 μm)	0.21	2.646	156	2.5	2.752	50 ± 5
NM 10 (3 μm)	0.44	2.633	169	3	2.750	52 ± 5

TABLE 8

Luminescence data for selected ZnSe:Te samples on GaAs(100).

ZnSe and must, therefore, be induced by the Te doping. Since the concept of isoelectronic traps was invoked orginally to described the PL emssion associated with the GaP:N system, it is instructive to see whether such a description is valid here.

The central factor when discussing inter-impurity recombinations involving isoelectronic species is that the isoelectronic trap is neutral in the absence of additional electronic particles. Thus in the present case the recombination of an electron bound to a donor with a hole bound to a Te isoelectronic trap, will result in no coulomb contribution to the DAP peak energy, ie $E_C = 0$. The pair transition energy, E(h) is then given by

$$E(ph) = Eg - (E^I_{Te} + E_D) = Ep \quad (Ep \sim O)$$

where Eg is the band gap of ZnSe, E_D is the donor binding energy in ZnSe and E^I is the binding energy of the Te isoelectric trap. E_p is a polarisation term, very small for normal r and is, therefore, neglected ($Ep \simeq O$). (r is the inter impurity, i-D, separation. Application of this equation yields

$$E^I_{Te} = 35 \text{ eV for sample NM 8.}$$

Since E_C is the major factor dispersing the energies for i-d pairs of different separations, a much narrower zero phonon line would be expected for i-D pairs than for normal D-A pairs, as is indeed observed. By analogy with the case of GaP:N, (C, Mg, Zn or Cd) described by Dean[10], one could postulated that the undulatory structure could be due to excitons bound to Te, but peturbed by nearby donors. (Undoped films had $n300K \sim 5 \times 10^{17}$ cm^{-3}). Thus each undulation peak could be due to a specific shell of donors measured from a given Te trap. If each undulation peak contained a large number of unresolved sharp pair lines, an overall modulation of the intensity envelope of these lines would account for the undulations. That is the exciton on Te would see a neutral donor a particular distance r away which would produce an increase in binding energy.

Since the binding energies of electrons at shallow donors in ZnSe (~26 meV) is greater than the binding energy of an electron to the hole at Te (4-5 meV), forming a bound exciton, one would predict that the (i-d) pair spectrum would be significant at low temperatures because thermalisation of the electrons out of the pair to form excitons would not occur. However, a number of factors stand agains this interpretation of the broad undulating

emission band. Most importantly, it must be remembered that a hole is believed to be trapped by the Te atom first, and because of its large binding energy (40 to 50 meV) is unlikely to intereact stongly with distant tellurium atoms. Additionally, the large extent of the undulation peak (500 meV wide) suggests an alternative mechanism is involved in the formation of the undulations, samples NM9 (0.21 at % Te) and NM10 (0.44 at % Te). Figs 8b and 8c respectively both exhibit PL spectra dominated by broad, but structured emission bands shifting to lower energy and broadening further with increase in Te concentration.

The PL spectrum of NM 9 (0.21 at % Te) at 77 K Fig 8d, reveals a broad peak centred at 2.552 eV, Stokes shifted by some 200 meV from where one would expect (D°,h) to occur from the temperature dependence of the free exciton band gap. However, at room temperature (290.6 K), Fig 8e, the same sample has a PL emission band peaking at 2.6957 eV where one would expect band to band recombination in undoped ZnSe. Clearly, whatever is responsible for the 10K and 77 K luminescence is quenched between 77 K and room temperature. The remarkable feature of the 77 K luminescence is its intensity, only 0.6x weaker than that obtained at 10 K, and its great width (~290 meV).

Reznitsky et al[8] and Lee et al[9] have attributed such a broad low temperature emission band in ZnSe-ZnTe alloys, grown from the bulk, with small x (1 at % %) as originating from the recombination of an exciton trapped at an isolated tellurium atom on a Se site. Such an exciton would have a binding energy of 40-50 MeV as can be seen from Table 8. The same authors also observe a lower energy band which they believe results from trapping by two tellurium atoms on nearest-neighbour Se sites. Thus there is the possibility of trapping by Te atoms paired on next-nearest neighbour sites and so on, giving rise to bands centred between those mentioned. Such a mechanism would explain the shift of the emission band with increase in Te concentration that is observed from NM 8 to NM 10. Since only broad bands envelope the phonon replicas, for NM 9 and NM 10, it would suggest that large local lattice relaxation accompanies single Te site occupation[11] (In general, electronic transition will contribute both a broad multi-phonon componenet and a sharp zero-phonon line to the luminescence spectrum, where the relative intensities are determined by the strength of the electron-phonon coupling[12].) The Huang-Rhys factors in Table 8 confirm that strong electron-phonon coupling is taking place. (Deep level emission has S

factors ~5). Thus the emission band at around 2.75 eV, hereafter referred to as E(Te_1), involves the emission of at least six LO phonons (Figures 8a-c).

Explanation of the temperature dependence of the luminescence features is deferred to the next section, where more data is available on the optical processes involved. The bound exciton model does seem more appropriate than the DAP model in explaining the observed features so far, and this hypothesis is substantiated further by the data on $ZnSe_{1-x}Te_x$ grown on InP (100). The binding energies of the Te, bound excitons are also in good agreement with the values obtained by Yao[5] et al for LPE grown $ZnSe_{1-x}Te_x$.

3. Growth and Characterisation of $ZnSe_{1-x}Te_x$ on InP(100)

INTRODUCTION

$ZnSe_{1-x}Te_x$ is a promising material for light emitting devices (blue to yellow) because of its large direct bandgap and for growth on InP substrates, lattice matching occurs for x = 0.46 at room temperature. Additionally, since ZnSe is produced intrinsically n-type whilst ZnTe is produced p-type, and it is very difficult to achieve type conversion of both materials, the system offers the prospect of ambipolar conductivity in an amphoteric solid solution and hence the possibility of p-n heterojunction formation. The following work was carried out to obtain preliminary data on the $ZnSe_{1-x}Te_x$ system.

RESULTS AND DISCUSSIONS

Growth

$ZnSe_{1-x}Te_x$ epilayers were grown on InP(100) substrates using the growth conditions listed in Table 9. The InP substrates (n-type) were baked out prior to growth in the range from 400°C to 500°C, following on from the work described in Section 1.

A large number of samples were grown but only the properties of a selected few will be discussed in detail. Once again difficulties encountered with the removal and disposal of the tellurium reactor by-products, restricted the range of flow conditions and DIPT bubbler temperatures that could be used. The result is that only Te concentrators of up to 3.2 at.% could be produced. In all of this work auxiliary heating of the DIPT inlet line was carried out (to 90 °C) to prevent premature condensation of the rather involatile DIPT. The growth rates obtained ranged from 4 $\mu m hr^{-1}$ to 12$\mu m hr^{-1}$ depending upon T_g and Te content. Resulting layers were generally 2-6 μm thick.

Total hydrogen flow rate (cm^3/min)	1600
Hydrogen flow rate through DMZ bubbler (cm^3/min)	7.5 - 16.7
Temperature of DMZ bubbler (°C)	-17 to -18
Hydrogen flow rate through DIPT bubbler (cm^3/min)	14 - 44.1
Temperature of DIPT bubbler (°C)	24 - 50
Flow rate of 5% H_2Se/H_2 (cm^3/min)	26.9 - 80.7
VI/II ratio	4
Growth temperature, Tg, (°C)	280 - 500

TABLE 9

Growth Conditions for $ZnSe_{1-x}Te_x$ Layers on InP(100)

Optical Microscopy

The surfaces of the $ZnSe_{1-x}Te_x$ films appeared rough, grainy and dull to the naked eye. Phase contrast microscopy revealed a pronounced dependence of the surface morphology on both growth temperature and Te content, with the relatively best surface morphologies being obtained at lower growth temperatures, around 280 °C and in the layers containing little Te ≤1.0 at %. In all cases, however, the morphologies were inferior to those obtained for ZnSe layers grown on InP(100) under otherwise identical growth conditions.

Figure 9a shows an optical photomicrograph of a $ZnSe_{1-x}Te_x$ (x = 0.30 at.%) layer, NM12, grown at 280 °C and although the surface is somewhat rough,

with hillocks, it is far superior to that obtained for a layer, NM17 (x = 2.45 at.%) grown at 450 °C, see Figure 9b. This layer exhibits an extremely grainy structure, appearing almost amorphous. Indeed the structural properties of these layers, discussed next, confirm these suspicions. The reason for these effects is unknown at present, but may possible involve adduct formation of DMZ with DIPT or an insufficient supersaturation of Te in the vapour, ie. a certain critical DIPT concentration may be required before efficient Te lattice incorporation takes place. The former possibility is analagous to the TMI/PH_3 situation that used to exist in the III-V growth of InP.

Double Crystal X-ray Diffraction and EDAX Analysis

As Table 10 shows, the growth temperature and/or the amount of Te incorporated has a severe effect on the crystallographic properties of the $ZnSe_{1-x}Te_x$ layers. (Since the layers are all of comparable thickness, linewidth variations due to sample curvature should be minimal). Lattice mismatch decreases with increasing incorporation of Te as one would expect, but the variation of mismatch with Te content appears not to be a simple one. Other effects involving strain (thermal expansion mismatch) may also be important. As Figures 10a-e and Table 10 show, the incorporation of only a little Te, NM12 (0.03 at.%) causes a very large increase in the epilayer FWHM over that obtained for ZnSe at the same growth temperature, Table 4. The severity of this line broadening increases as the amount of Te is increased until for layers containing around 2.5 at.%, (NM17) the FWHM of the $ZnSe_{1-x}Te_x$ broadens to around 3800 arc seconds. The resulting diffraction signal is very weak and the layer is obviously polycrystalline tending towards an amorphous form. For higher levels of Te, NM18 (3.21 at.% no alloy diffraction signal is obtained indicating an amorphous film. Growth at a higher temperature under otherwise identical growth conditions leads to an improved alloy crystallinity and a small increase in Te content, NM12 and NM13. This is presumably due to an improvement in the crystal quality of the ZnSe host lattice with increasing T_g.

Sample no. layer thickness	Tg/(°C)	at % Te	FWHM $ZnSe_{1-x}Te_x$ /arc sec	FWHM InP /arc sec	Mismatch
NM 12 (3 μm)	280	0.30	853	40	-3.8702×10^{-2}
NM 13 (3 μm)	370	0.45	410	26	-3.5149×10^{-2}
NM 14 (2.5 μm)	400	1.59	1113	53	-3.3137×10^{-2}
NM 15 (2 μm)	450	1.68	2396	26	-3.3012×10^{-2}
NM 16 (3 μm)	350	1.81	514	31	-3.6879×10^{-2}
NM 17 (2 μm)	450	2.45	3762	27	-3.2068×10^{-2}

TABLE 10

Structural and Compositional Data For $ZnSe_{1-x}Te_x$ on InP(100)

The reason for the degradation in alloy structural quality with increasing Te content is unknown at present, but may involve undesirable side reactions in the deposition process as discussed earlier.

Photoluminescence Properties

The PL spectra of $ZnSe_{1-x}Te_x$ layers grown on InP containing small atomic fractions of Te (< 1 at %) are very similar to those grown on GaAs(100) exhibiting a broad, dominant emission peak at around 2.6 eV attributed to Te_1, NM13, Figure 11a. However, samples containing greater atomic fractions

of Te (<1 at,%), NM 14, NM 15 and NM 17, Figures 11b-d exhibit spectra dominated by a peak of similar lineshape, unresolved phonon structure, but downshifted in energy and centred around 2.50 eV to 2.45 eV depending upon the Te content. There is a progressive shift of this emission band to lower energy with increasing Te content. The lack of phonon structure does not permit an estimate of the exciton binding energy to be made for this band, indicating an increase in the strength of electron-phonon coupling[11]. However, tentative estimates of the exciton binding energy have been made using the data of Yao et al[5]. These authors quote a binding energy of around 250 meV for the exciton associated with a band centred at 2.48 eV. Thus the binding energies of the excitons involved here would be suggested to be > 250 meV for samples NM 14 and NM 15. Lee et al[4] and Yao et al[5] have attributed this emission band to recombination of excitons at Te_n (n>2) clusters and it is believed that a similar assignment can be made here. The emission bands are all broad with FWHM's of the order of 200 meV.

The presence of Te_n clusters would imply that an inhomogenous broadening component is superimposed on the homogenous electron-phonon broadening component. Fluctuations in either the number or relative positions of Te atoms in a cluster will modify the individual values of the binding energies strongly energy dispersing the exciton lifetimes. Such dispersion arises due to a decrease of the exciton oscillator strength with increased binding energy.[8] As x is increased, see Table 11, the intensity of the band, due to clusters, increases at the expense of that at single Te atoms. A shift from E(Te,) for sample NM 13 (0.45 at % Te) to E (Te_n) for sample NM 14 (1.59 at % Te) exemplifies this trend. E(Te_1) is completely absent in NM 14.

Yao et al[5] have attributed this to efficient radiative transfer involving excitons at Te_1 and Te_n sites. They have shown that the emission spectrum from excitons at Te_1 sites strongly overlaps the excitation spectrum for excitons at Te_n clusters. Thus, the emission occurs preferentially from clusters with n>2 except at very low tellurium concentrations. Strong exciton localisation at these Te_1 and Te_n sites also explains why the 10 K PL spectra are dominated by Te related emissions. Spatial migration of energy will be suppressed by strong localisation, revealing itself by the suppression of all recombination channels except those involving radiative recombination of strongly bound excitons.[8]

Sample no. Layer Thickness	at % Te 0.1%	Te emission peak E^{Te} (eV)	Stokes shift (meV) $\Delta E_S = E^{ZnSe} - E^{Te}$	Huang-Rhys factors, S	Zero-phonon energy E_O (eV)	Exciton binding energy $\Delta E^{Te} = E^{ZnSe} - E_O$ (meV)
NM 13 (3 μm)	0.45	2.638	164	2.5	2.756	46 ± 5
NM 14 (2.5 μm)	1.59	2.460	342	-*	-*	-
NM 15 (2 μm)	1.68	2.453	349	-*	-*	-
NM 17 (2 μm)	2.45	2.507	295	-*	-*	-

TABLE 11

Luminescence data for selected $ZnSe_{1-x}Te_x$ samples grown on InP(100)

* Peak phonon structure is unresolved. Error in estimated values of Eo is very large. (~ 50 meV). Unable to calculate E^{Te} from emission spectrum for these samples.

If one assumes that Te atoms are randomly distributed on anion sites in $ZnSe_{1-x}Te_x$, a simple binomial probability can be evaluated for the appearance of Te_n clusters. As x increases as well as Te_1, Te_n will appear with increasing probability where any given Te atom has (n-1) Te atoms on the twelve nearest neighbour anion sites.[13]

Thus we get

$$W_n(x) = x \binom{12}{n-1} x^{n-1}(1-x)^{12-(n-1)}; \quad n = 1,2,....13$$

assuming equal site probability for Se and Te on anion sites.

Figure 12 shows cluster probability normalised by $W_n(x)$ as a function of x. Indeed as Figure 13 shows, Te_2 clusters have a reasonable degree of probability, admittedly for a large x (> 0.1). However, as Table 11 indicates, Te_2 clusters can be detected optically well below the region where $W_n(x)$ should become significant (x 0.154), indicating a considerably more complex situation.

The reduction of the band gap with increasing x shifts all of the exciton bands to lower energy. However, the shift of these bands does not follow the variation of the $ZnSe_{1-x}Te_x$ alloy band gap, see Figure 14. Here Eg(x) for $ZnSe_{1-x}Te_x$ is given by

$$E_g(x) = x\,E_{ZnTe} + (1-x)\,E_{ZnSe} - bx\,(1-x)$$

where the 'bowing' factor b(= 1.23 eV) and the values E_{ZnSe} = 2.82 eV and E_{ZnTe} = 2.39 eV are taken for the ZnSe and ZnTe band gaps respectively.[14]

Further support for the Te cluster model comes from the temperature dependence of the PL spectra.

The variation of the PL emission with temperature for sample NM 14 (1.59 at %) is shown in Figures 15a-f. As the sample temperature is increased from 10K upwards the Te_n emission band shifts downwards in energy from 2.463 eV at 30 K to 2.431 eV at 100 K. Moreover, the PL signal intensity drops only by a factor of 16% over this temperature range. The radiative efficiency of this band is substantially higher than (D,h) emission in nominally undoped ZnSe or ZnTe. As the temperature is increased further from 120 K to 220 K the Te_n emission band shifts from 2.416 eV to 2.34 eV. Over this temperature range, however, the radiative efficiency, , the band drops only 11% of the value at 10 K. From 220 K up to room temperature, the emission band

increases slightly up to 2.385 eV and is strongly broadened by thermalisation. Now is only 3% of the value at 10K but still signigicantly larger that as a fraction of the 10K luminescence involving (e,h) recombination in nominally undoped ZnSe. Interestingly, however, the room temperature emission band appears 300 eV below where one would expect (e,h) recombination in ZnSe. The reason for the upshift in peak energy between 220 K and room temperature is discussed later.

These temperature dependent results can be understood using the exciton extrinsic self-trapping model of Lee et al.[9] Self trapped excitons or strongly localised excitons have a higher radiative efficiency than either free or standard Wannier excitons, because of their very large effective translational mass, preventing migration towards non-radiative recombination centres. Lee et al[9] have used a configurational coordinate diagram to explain the spectral changes occuring under band to band excitation as the sample temperature is raised. The schematic diagram they used is shown in Figure 16. It appears that two energy barriers E_1 and E_2 separate free and Te_1 an Te_n(n 2) bound excitons respectively. At low temperatures, T<50 K (E_{Bx} ~ 4-5 meV) excitons initially created by the laser beam will be captured and recombine around the numerous Te_1 sites (x < 1 at %), which have a small energy barrier, giving rise to the E(Te_1) luminescence band, sample NM 9 (x = 0.21 at %), Figure 8b, process a in Figure 16. As the temperature is increased, excitons localised at Te_1 sites are thermally activated back over the barrier ΔE, (process b, Figure 16) regenerating mobile free excitons which in turn become increasingly captured at Te_n (n = 2) sites (process c, Figure 16) leading to the E(Te_n) emission band for sample NM 9 at 77 K, Figure 8d. At higher temperatures, T 100 K, the reverse process (d, in Figure 45) over barrier ΔE_2 takes place. Thus at room temperature (e,h) recombination predominates, see Figure 8e for sample NM 9. Delocalisation of excitons will increase the diffusion length of energy migration, leading to an increase of the non-radiative recombination rate and consequently to a reduction in , (0.8% of I_x at 10 K).

A similar mechanism would appear to be operative in the samples with a higher Te content, NM 14 (1.59 at % Te) and NM 15 (1.68 at % Te). In these cases, although the emission due to Te_n clusters is displaced to lower energies compared to Te_2 peak energies given by Yao et al[5]. Due to a dispersion of exciton lifetimes as discussed earlier, processes analogous to

c and d in Figure 16 are occurring. The temperature dependence of the PL spectra for sample NM 14 (1.59 at % Te) is shown in Figure 17. The temperature dependence of the free exciton band gap for ZnSe is also shown. It is obvious that for temperatures from 10 K to around 150 K there is an approximately constant Stokes shift (~340 ± 15 meV) of the $E(Te_n)$ band below the free exciton band gap. That is the $E(Te_n)$ band follows the shrinkage of the ZnSe band gap with temperature not the alloy, $ZnSe_{1-x}Te_x$ band gap, confirming that in-gap states are controlling the luminescence behaviour. However, at temperatures >150 K one would expect these Te_2 centres, with a binding energy 250 meV to be dissociated and the luminescence quenched. This is indeed observed. For 150 K < T < 220 K process d in Figure 16 has emptied the Te_2 centres and the Stokes shift has increased (~ 400 meV) indicating that emission from a Te_n centre of larger binding energy (~ 380 meV) indicating that emission from a Te_n centre of a larger binding energy (~380 meV) is taking place. As the temperature increases further >220 K up to room temperature, the Stokes shift changes again (~ 320 meV) indicating that yet another Te_n centre of larger binding energy (~500 meV) is involved).

It is also worth mentioning that the internal electronic energy of the localised excitons is on the same order as that of free excitons at rest. This conclusion is reached by analysing the position and width of the $E(Te_2)$ band using the following relation.[15]

$$D^2 = 11\, E_R kT$$

Where D is the width (FWHM) of the emission band, E_R represents the elastic energy stored in the equilibrium position of the distorted lattice and T is the lattice temperature. At sample temperatures above 150 K, Figure 15f, this yields E_R ~300 meV. This value is comparable to the measured Stokes shift between $E(Te_2)$ and the free exciton (~ 225 meV). As Figure 16 shows, this indicates that free and bound excitons (at Te_2) must have very similar electronic energies, despite the large observed Stokes shift.

4. Growth and Characterisation of ZnTe on InAs(100)

In order to investigate whether or not growth of the Te rich alloy could be accomplished, ie growth of $ZnSe_{0.1}Te_{0.9}$ lattice matched to InAs(100), a few

layers of ZnTe were grown on InAs under varying conditions.

The major parameters investigated were the effects of Tg and VI/II ratio on the film properties and the layers were characterised by optical microscopy, double crystal X-ray diffraction and PL. Unfortunately, all the layers grown at temperatures from 280 °C to 400 °C at VI/II ratios from 1.5 to 4 exhibited very poor morphologies and appeared amorphous. No PL signal or X-ray diffraction signal could be obtained. The surfaces produced are very similar to those of ZnSe grown at comparable temperatures but under Zn rich conditions (ie VI/II ratios from 1 to 1/4). The surfaces show evidence of pitting, inclusions and clusters indicating a deficiency of Te in the deposited layers.

Once again safety considerations prevented the use of high Te flow rates but layers grown at 400 °C at a VI/II ratio of 6 exhibited greatly improved morphologies. Although smooth and shiny surfaces could be produced, the resulting layers were too thin for adequate characterisation to be performed (necessity for short growth times). However, Figure 18 shows the double crystal X-ray diffraction pattern from a ZnTe layer $< 0.2\,\mu m$ thick. For such a thin layer the FWHM of the ZnTe is very large, 2026 arc seconds (InAs substrate FWHM - 35 arc seconds), and the signal is very weak and only just resolvable. A PL spectrum of the same layer, indicates just a scattering component of the laser line.

REFERENCES

1. N. Maung, Ph.D Thesis, University of Manchester, 1988.

2. N. Hunt, Ph.D Thesis, University of Manchester 1988.

3. M.J. Hill, B.K. Tanner, M.A.G. Halliwell and M.H. Lyons, J. Appl. Cryst., 18, 1985, 446.

4. S.B. Quadri, B.T. Janker, G.A. Prinz and J.J. Krebs, J. Vac. Sci. Technol. A, 6 (3), 1988 1526.

5. T. Yao, M. Kato, J.J. Davies and H. Tanino, J. Cryst. Growth, 86, 1988, 552.

6. S. Permogorov, A. Reznitsky, S. Verbin, G.O. Muller, P. Fogel and M. Nikiforova, Phys. Stat. Sol., (b)113, 1982,589.

7. W. Heimbrodt and O. Goede, Phys. Stat. Sol., (b)135, 1986, 795.

8. A. Reznitsky, S. Permogorov, S. Verbin, A. Naumov, Y. Korolstelin, V. Novozhilov and S. Prokov'ev, Solid St. Commun., 52 (1), 1984, 13.

9. D. Lee, A. Mysyrowicz, A.V. Nurmikko and B.J. Fitzpatrick, Phys. Rev. Lett., 58 (14), 1987, 1475.

10. P.J. Dean, 'Inter-Impurity Recombinations in Semiconductors', in Progress in Solid State Chemistry Vol. 8, Eds. J.O. McCaldin and G. Samorjai, p.1.

11. D.M. Roessler, J. Appl. Phys., 41 (11), 1970, 4589.

12. D.B. Fitchen in Physics of Color Centres, edited by W.B. Fowler (Academic Press, New York, 1968), p.293.

13. O. Goede, W. Heimbrodt, R. Muller, Phys. Stat. sol. (b), 105, 1981, 543.

14. J.J. Davies, Semicond. Sci. Technol., 3, 1988, 219.

15. Y. Toyozawa in Proceedings of the 16th Int. Conf. on Physics of Semiconductors, edited by M. Averous (North Holland, Amsterdam 1982); Y. Shinozuka and Y. Toyozawa, J. Phys. Soc. Japan, 46, 1979, 505.

LIST OF FIGURES

Fig. 7a Double crystal X-ray diffraction pattern for sample NM 8, (x = 0.0018).

Fig. 7b Same as Fig. 13 but for sample NM 9, (x = 0.0021).

Fig. 7c Same as Fig. 13 but for sample NM 10, (x = 0.0044).

Fig. 8a 10 K PL spectrum for sample NM 8, (x = 0.0018)

Fig. 8b " " " NM 9, (x = 0.0021)

Fig. 8c " " " NM 10, (x = 0.0044)

Fig. 8d 77 K " " NM 9, (x = 0.0021)

Fig. 8e 290.6 K " " NM 9, (x = 0.0021)

Fig. 9a Optical photomicrograph of the surface morphology for sample NM 12, (x = 0.003)

Fig. 9b Optical photomicrograph of the surface morphology for sample NM 17, (x = 0.0245).

Fig. 10 Double crystal X-ray diffraction for samples indicated

(a) NM 12 (x = 0.003)

(b) NM 13 (x = 0.0045)

(c) NM 15 (x = 0.0159)

(d) NM 16 (x = 0.0181)

(e) NM 17 (x = 0.0245)

Fig. 11 10 K PL spectrum of sample (a) NM 13, (x = 0.0045)
" " " (b) NM 14, (x = 0.0159)
" " " (c) NM 15, (x = 0.0168)
" " " (d) NM 17, (x = 0.0245)

Fig. 12 Normalised cluster probability for Te_n clusters (n = 1 to 5) as a function of Te content.

Fig. 13 Maximum cluster probability as a function of the number of Te atoms in a cluster.

Fig. 14 Photoluminescence peak energies for $ZnSe_{1-x}Te_x$ alloys and full line is the alloy optical band gap computed as a function of x.
- emission due to Te_1.
- emission due to Te_n. (n 2)

Fig. 15 PL emission spectra for sample NM 14 (x = 0.0159) at ...K.

(a) 30 K

(b) 69.7 K

(c) 120.2 K

(d) 180.2 K

(e) 230.0 K

(f) 290.4 K

Fig. 16 Schematic diagram etc as in figure Legend (from Lee et al).

Fig. 17 Temperature dependence of the free exciton band gap for ZnSe (Continuous line) and the Te_n (n = 2) emission band (boxes).

Fig. 18 Double crystal X-ray diffraction pattern from a ZnTe layer (0.2 μm thick), T_g = 400 °C; VI/II ratio = 6.

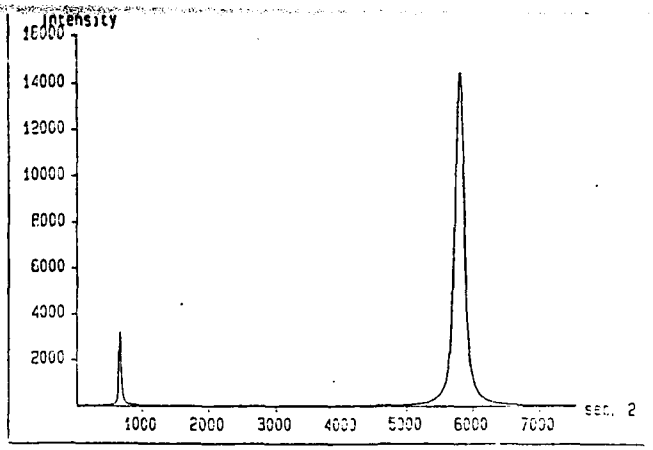

NM 1 Fig. 2a T_B = 600 °C

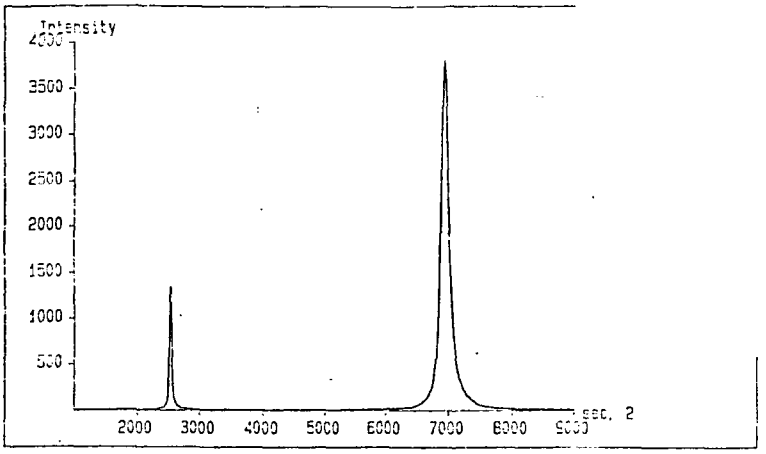

NM 2 Fig. 2b T_B = 400 °C

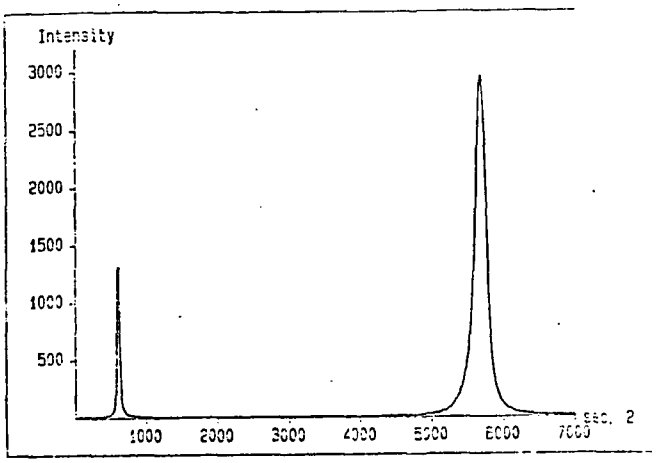

NM 3 Fig. 2c T_B = 500 °C

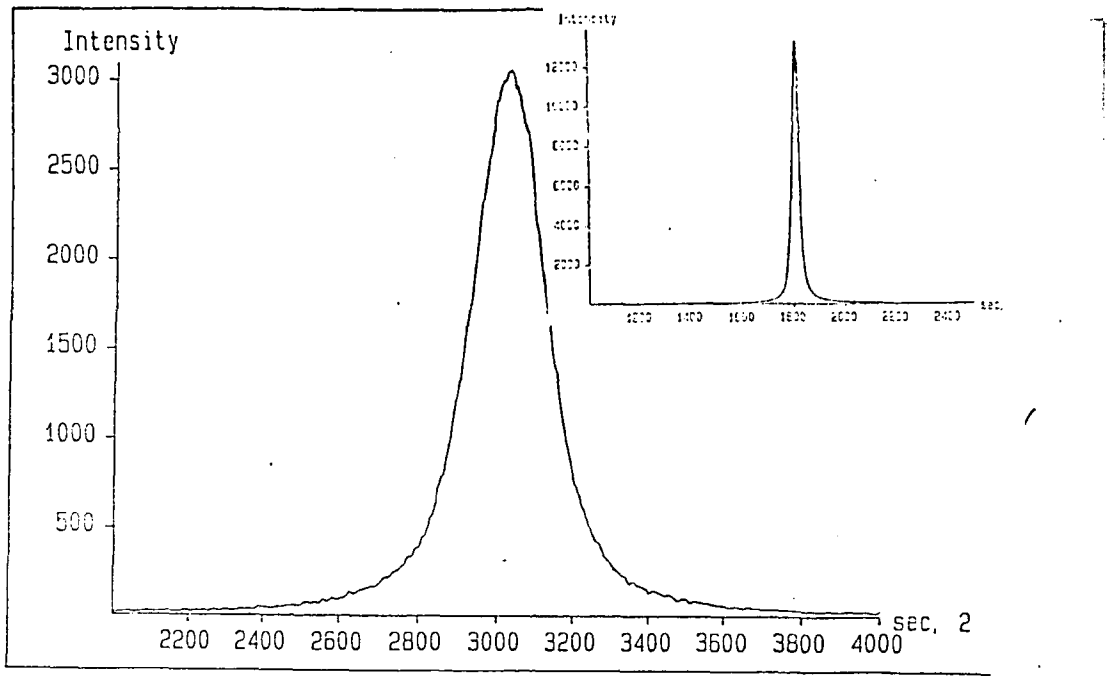

Fig. 3a Same as Fig. 2, but for sample NM 5, ZnSe/InAs(100).

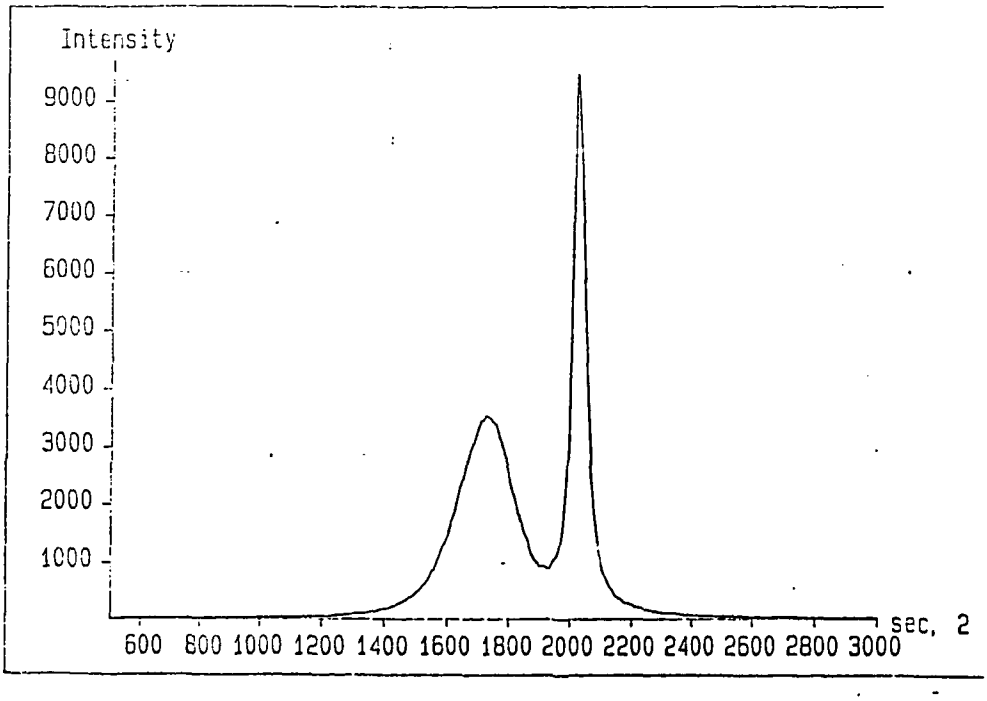

Fig. 3b Same as Fig. 2, but for sample NM 6, ZnSe/GaAs(100).

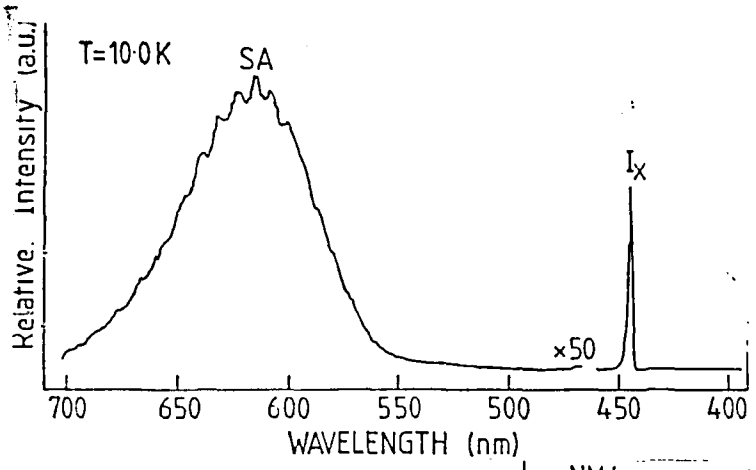

Fig. 4a

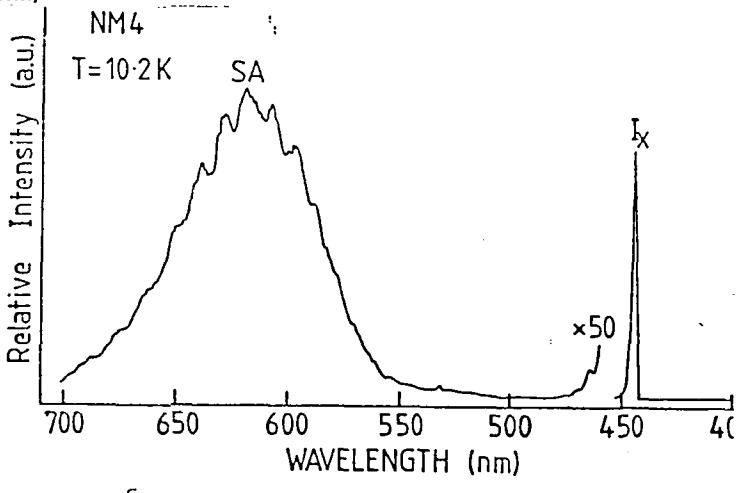

Fig. 4b

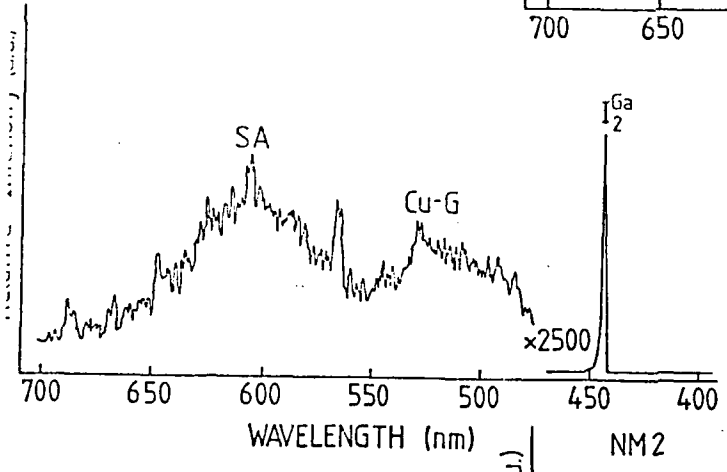

Fig. 4c

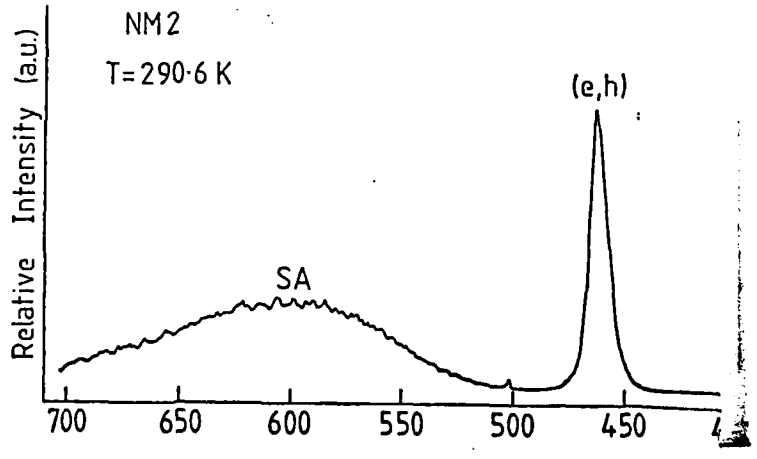

Fig. 4d

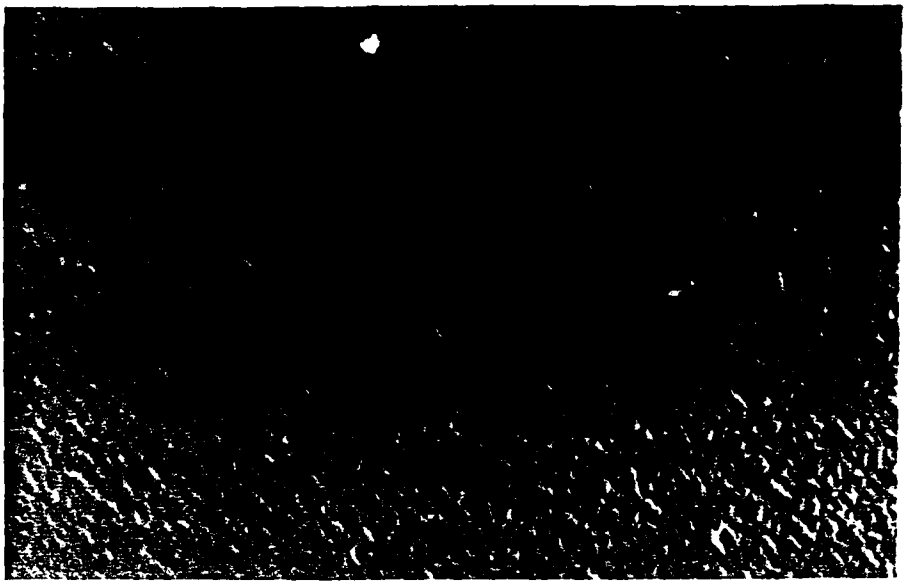

Fig. 5 Optical Photomicrograph of the Surface Morphology for Sample NM 10, (x = 0.0044) (x 1000)

6a

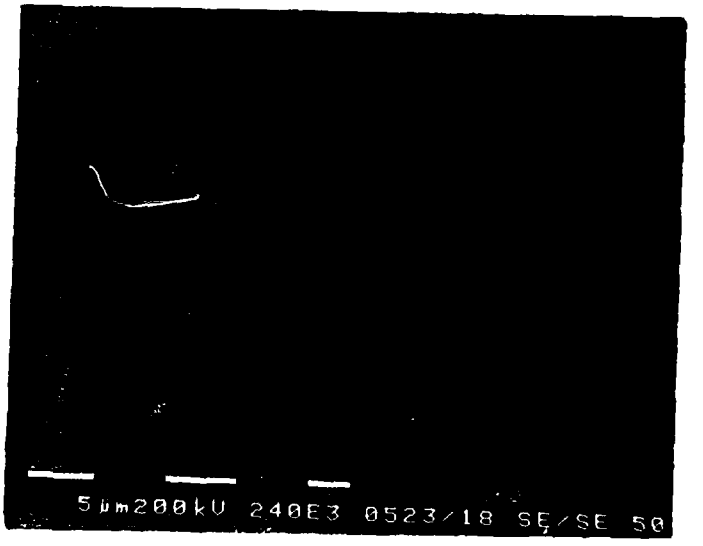

6b

Fig. 6 SEM Photomicrographs for the Surface Morphology and Cross Section of Sample NM 8, (x = 0.0018)

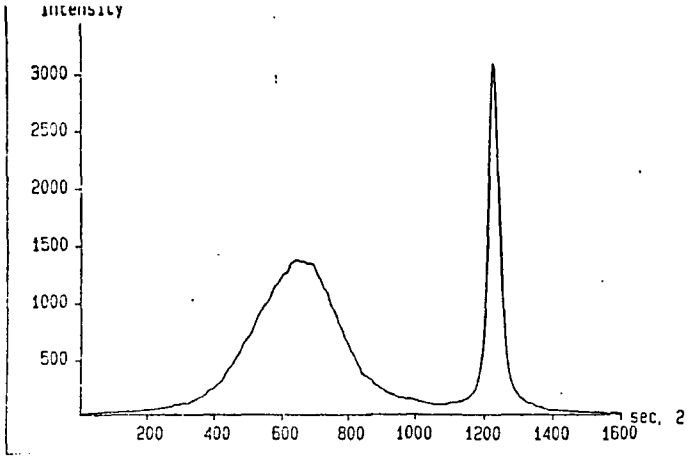

Fig. 7a Double crystal X-ray diffraction pattern for sample NM 8, (x = 0.0018).

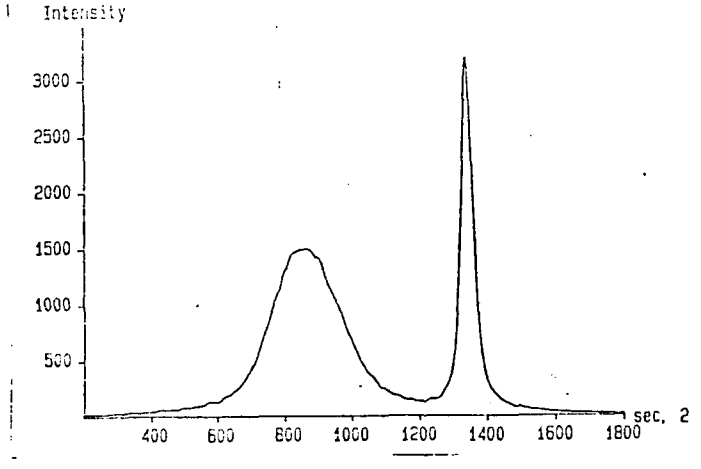

Fig. 7b Same as 7a but for sample NM 9, (x = 0.0021).

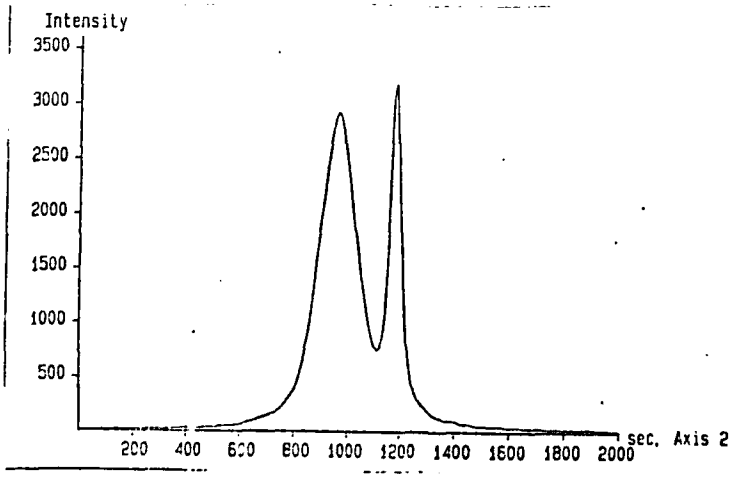

Fig. 7c Same as 7a but for sample NM 10 (x = 0.0044).

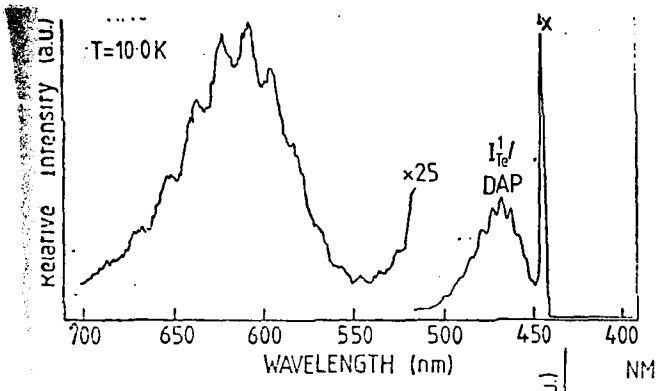

Fig. 8a

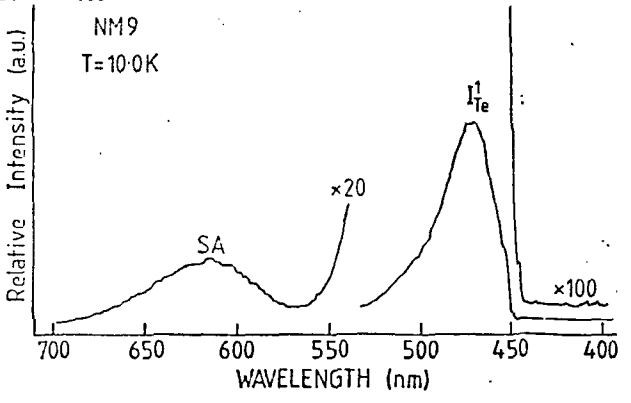

Fig. 8b

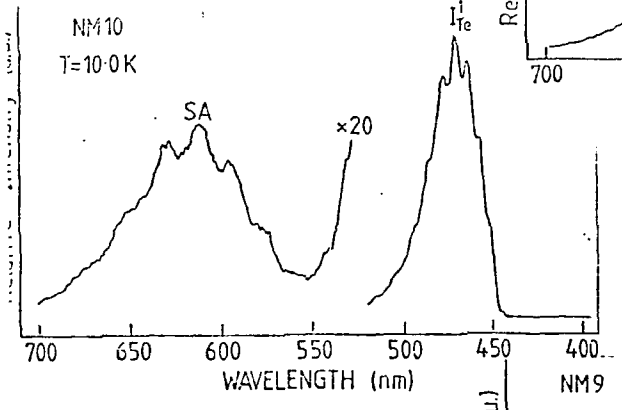

Fig. 8c

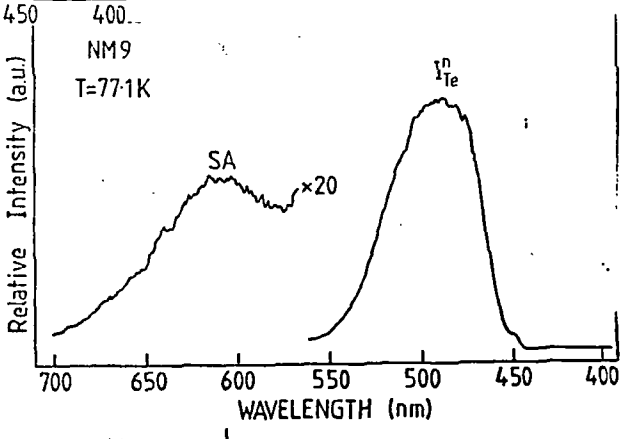

Fig. 8d

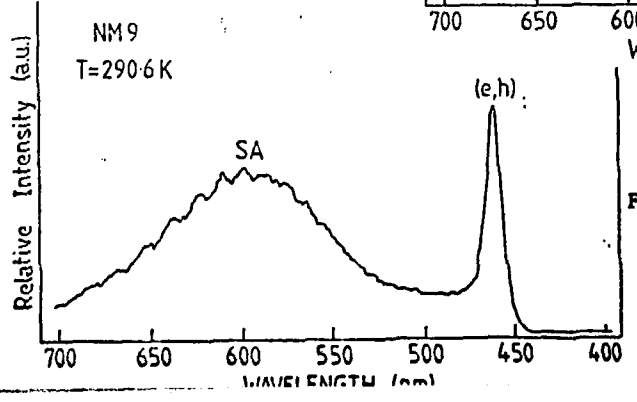

Fig. 8e

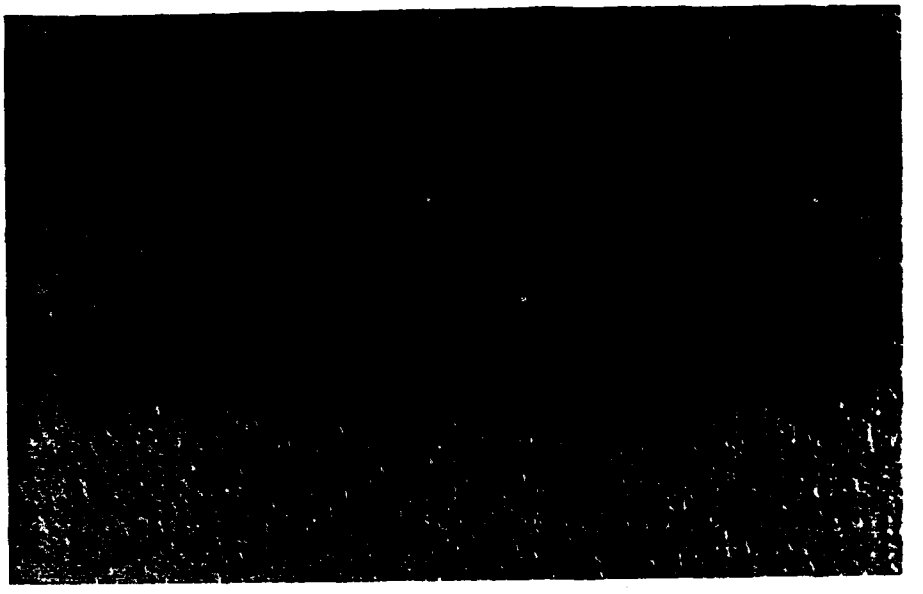

Fig. 9 Optical Photomicrograph of the Surface Morphology for Sample NM 12, (x = 0.003) (x 1000)

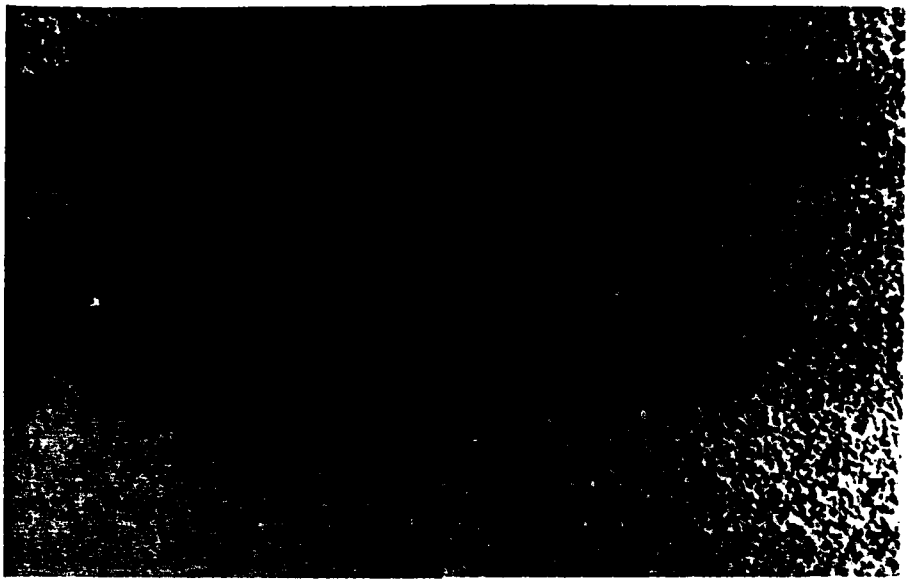

Fig. 9b Optical Photomicrograph of the Surface Morphology for Sample NM 17, (x = 0.0245) (x 1000)

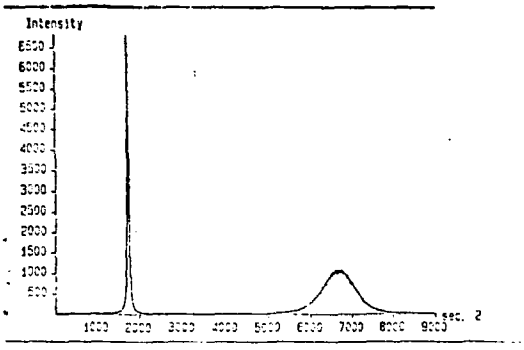

Fig. 10a NM 12 (x = 0.003)

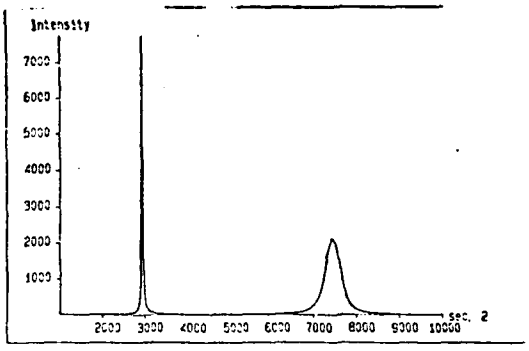

Fig. 10b NM 13 (x = 0.0045)

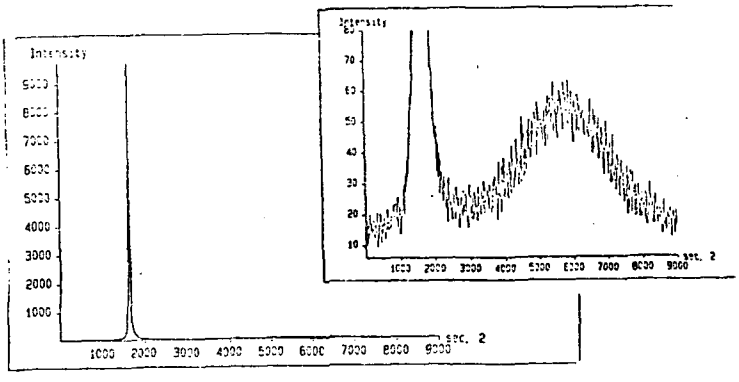

Fig. 10c Double crystal X-ray diffraction for samples NM 15 (x = 0.0159).

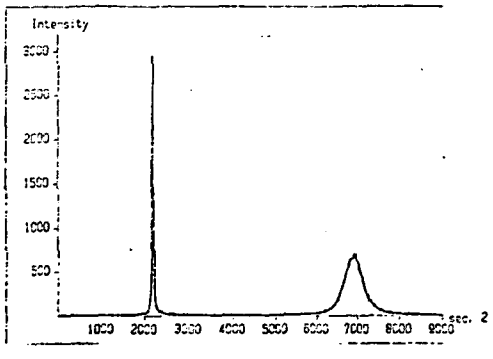

Fig. 10d NM 16 (x = 0.0181)

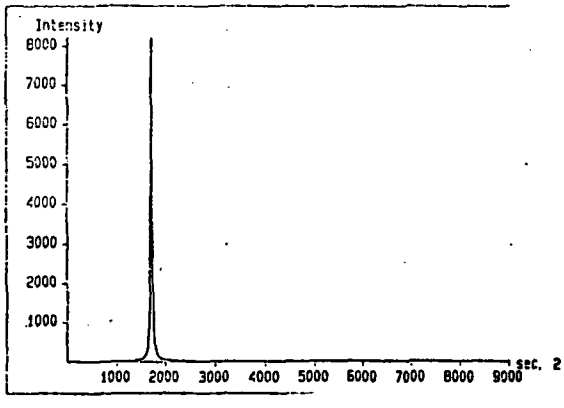

Fig. 10e NM 17 (x = 0.0245).

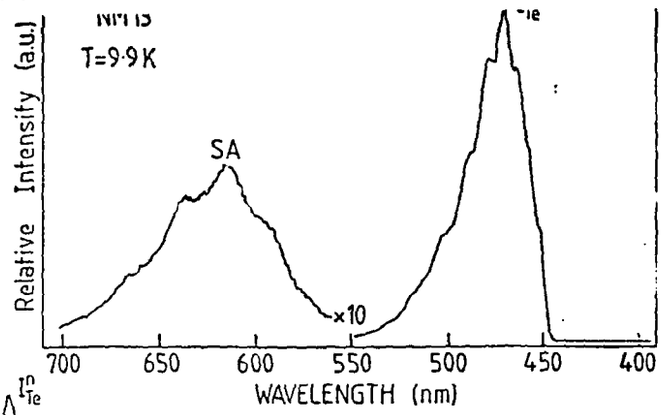

Fig. 11a

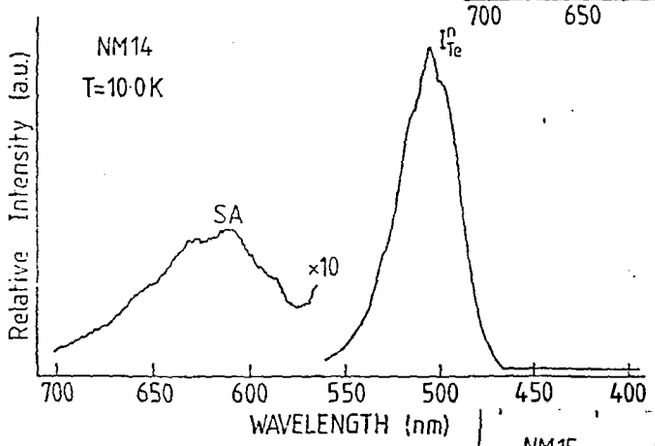

Fig. 11b

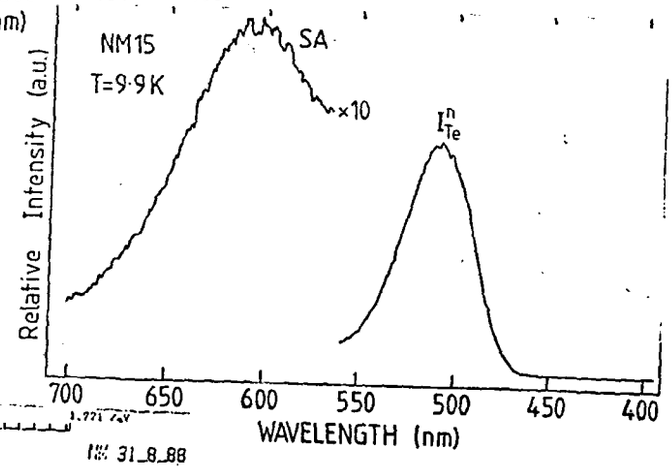

Fig. 11c

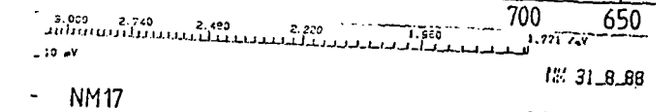

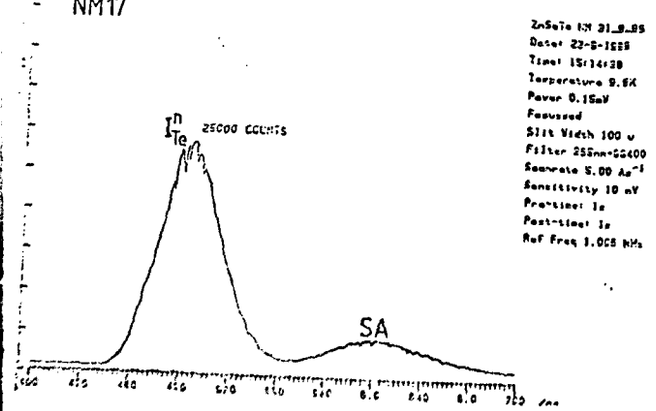

Fig. 11d

Fig. 12

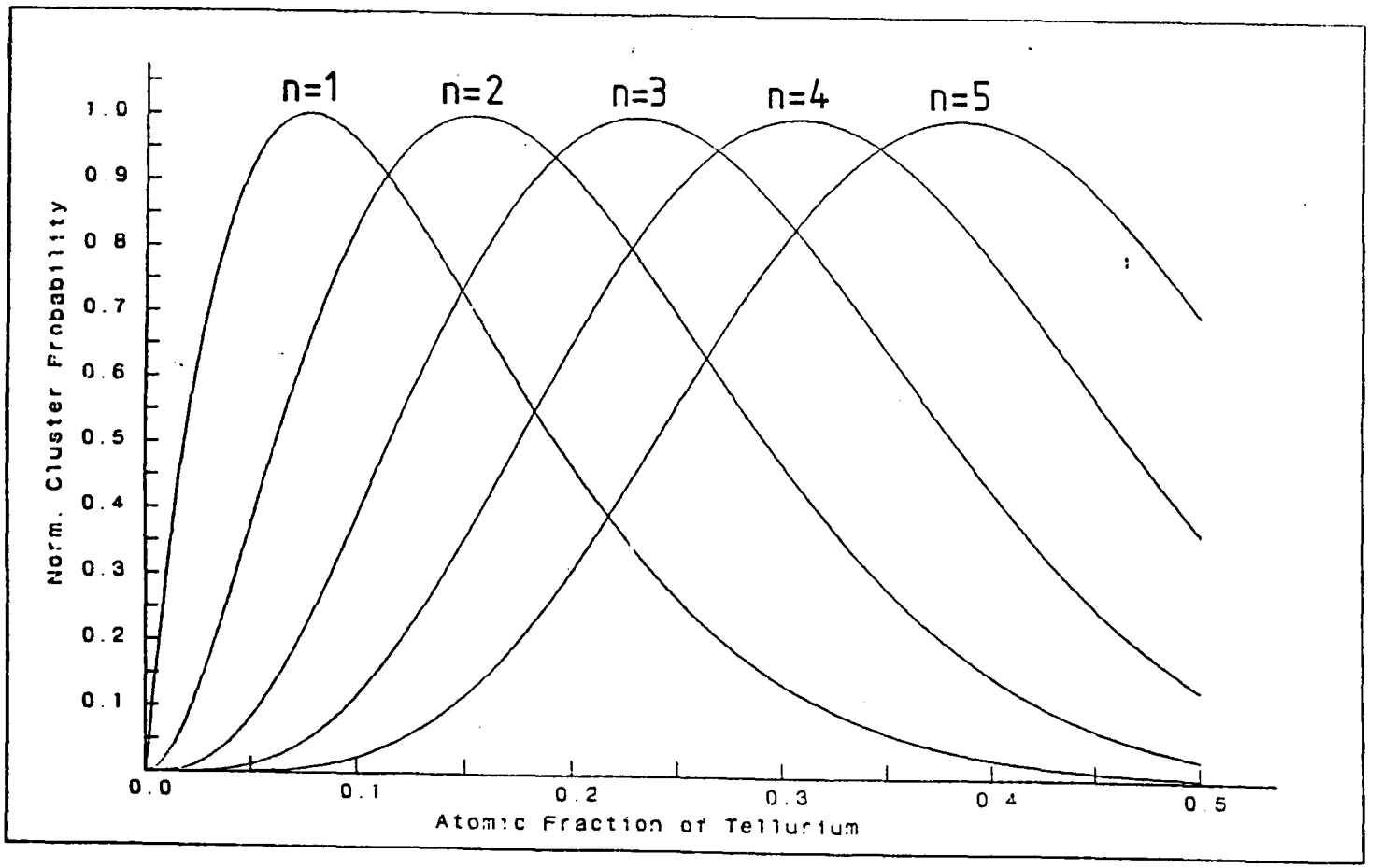
n=1
n=2
n=3
n=4
n=5
Norm. Cluster Probability
1.0
0.9
0.8
0.7
0.6
0.5
0.4
0.3
0.2
0.1
0.0
0.1
0.2
0.3
0.4
0.5
Atomic Fraction of Tellurium

Fig. 13

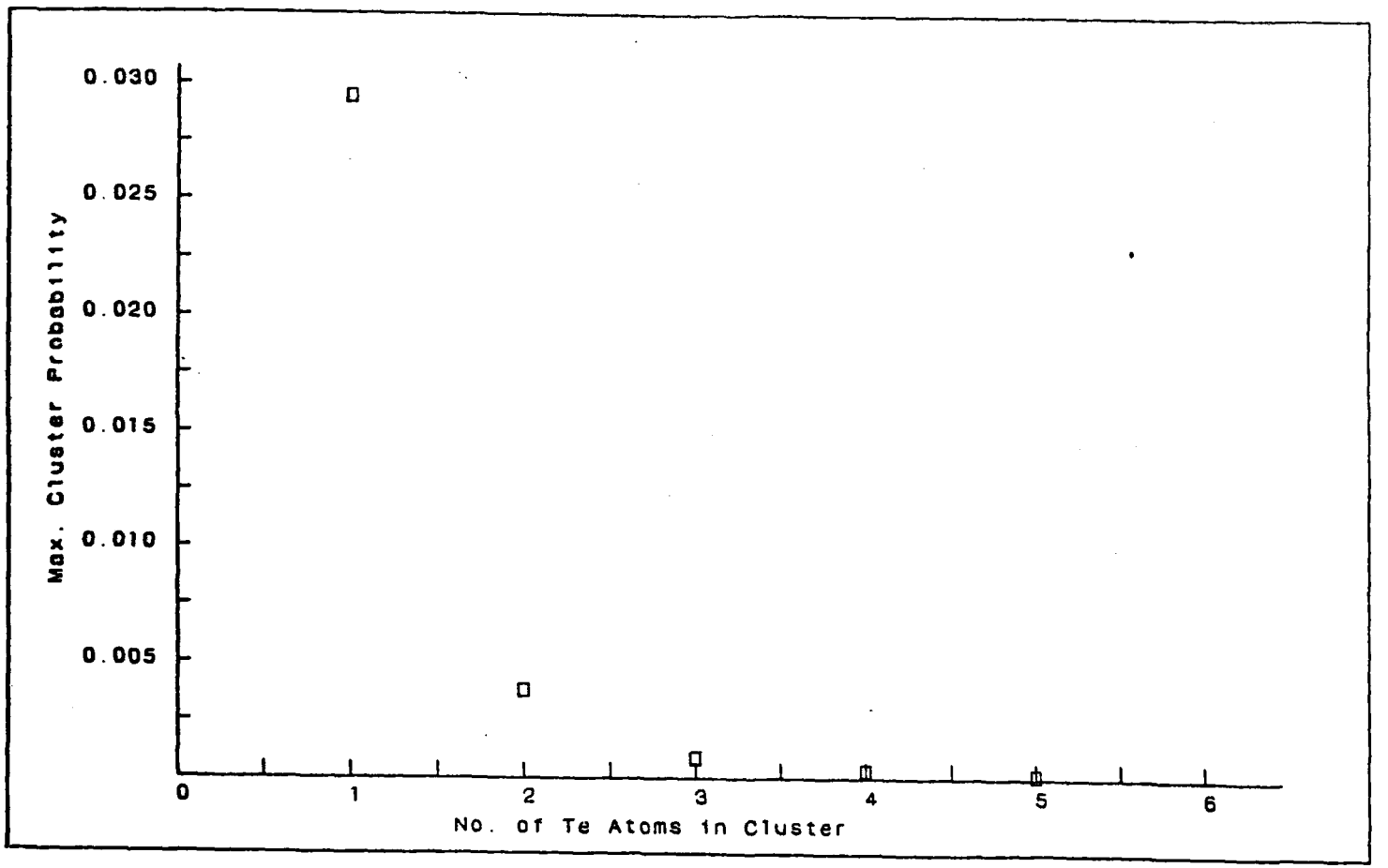
0.030
0.025
0.020
0.015
0.010
0.005
Max. Cluster Probability
0
1
2
3
4
5
6
No. of Te Atoms in Cluster

Fig. 14

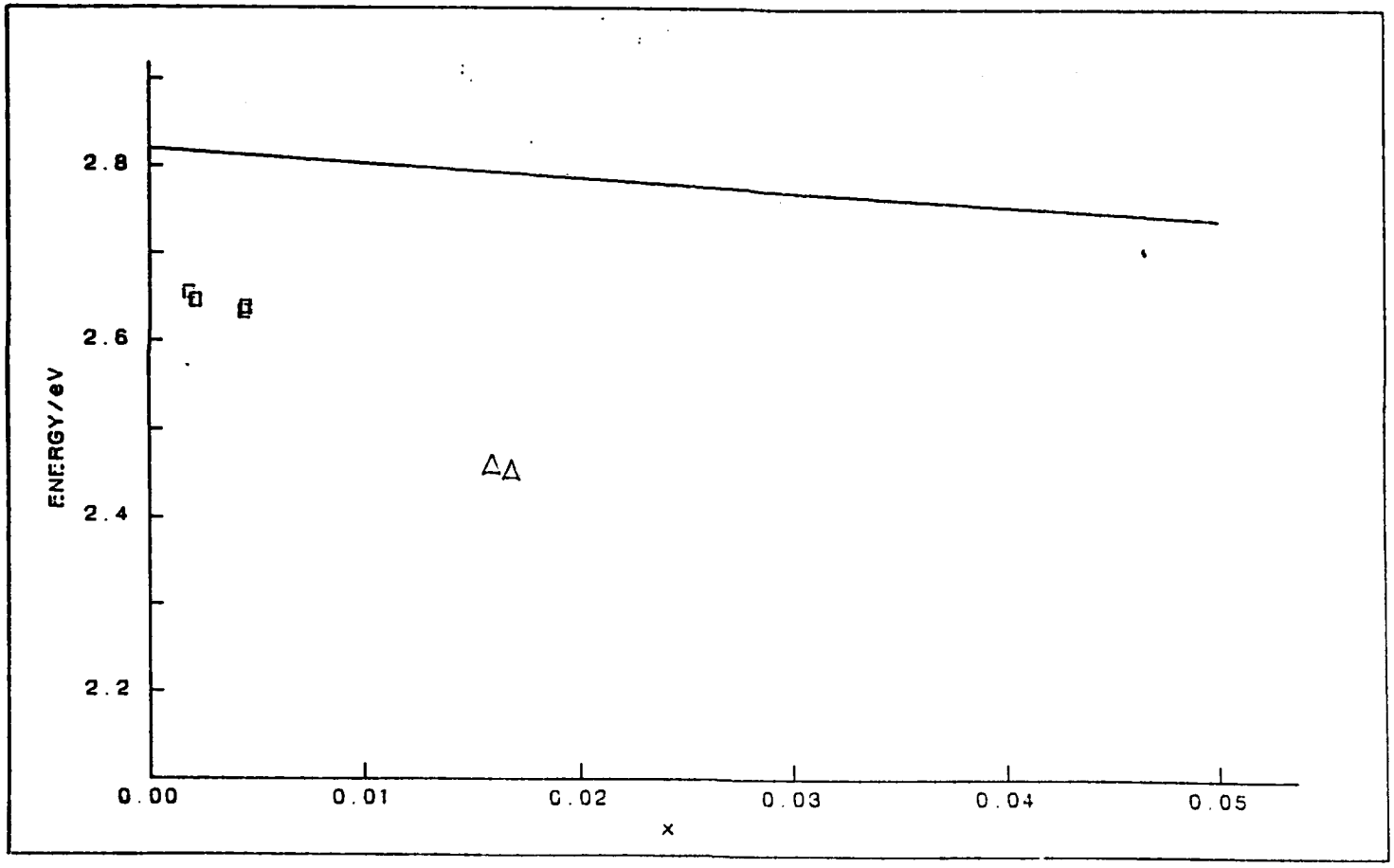

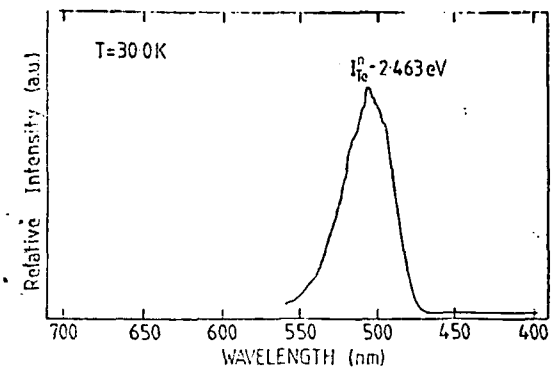

Fig. 15a

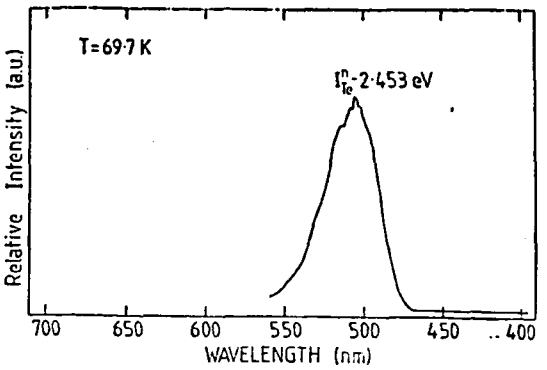

Fig. 15b

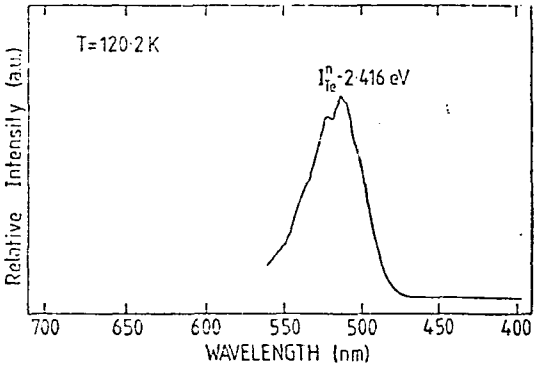

Fig. 15c

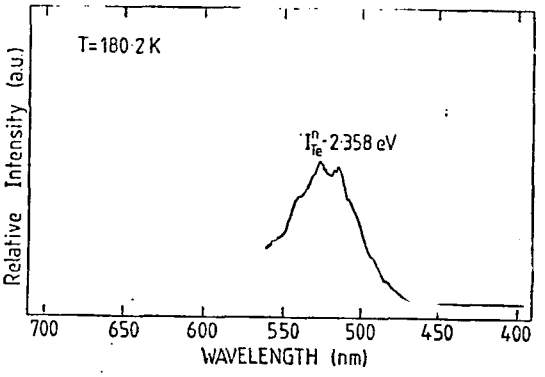

Fig. 15d

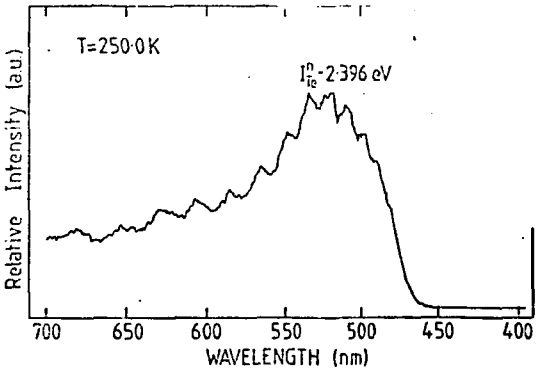

Fig. 15e

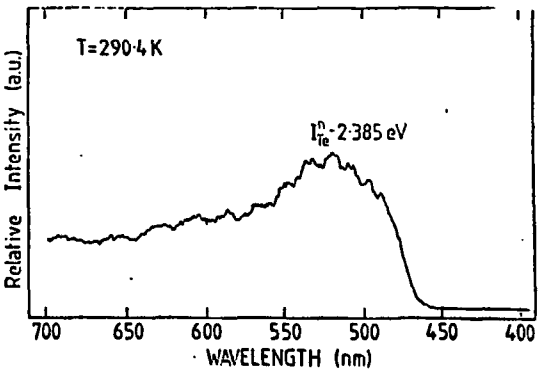

Fig. 15f

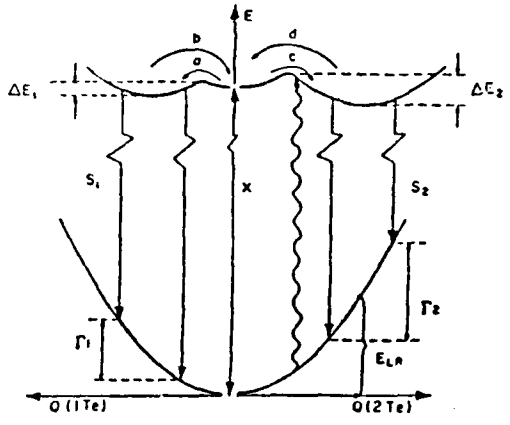

Schematic diagram of the model used in the discussion, showing the total energy of the system in the presence of an exciton (upper curves) and in the electronic ground state (lower curve). Q represents a configuration coordinate for a single Te site (left-hand side) or two nearest-neighbor Te atoms (right-hand side). X is for a free exciton at rest. Descending arrows depict the recombination from localized excitons, the ascending arrow the direct creation of an exciton self-trapped around two Te.

Fig. 16

Fig. 17

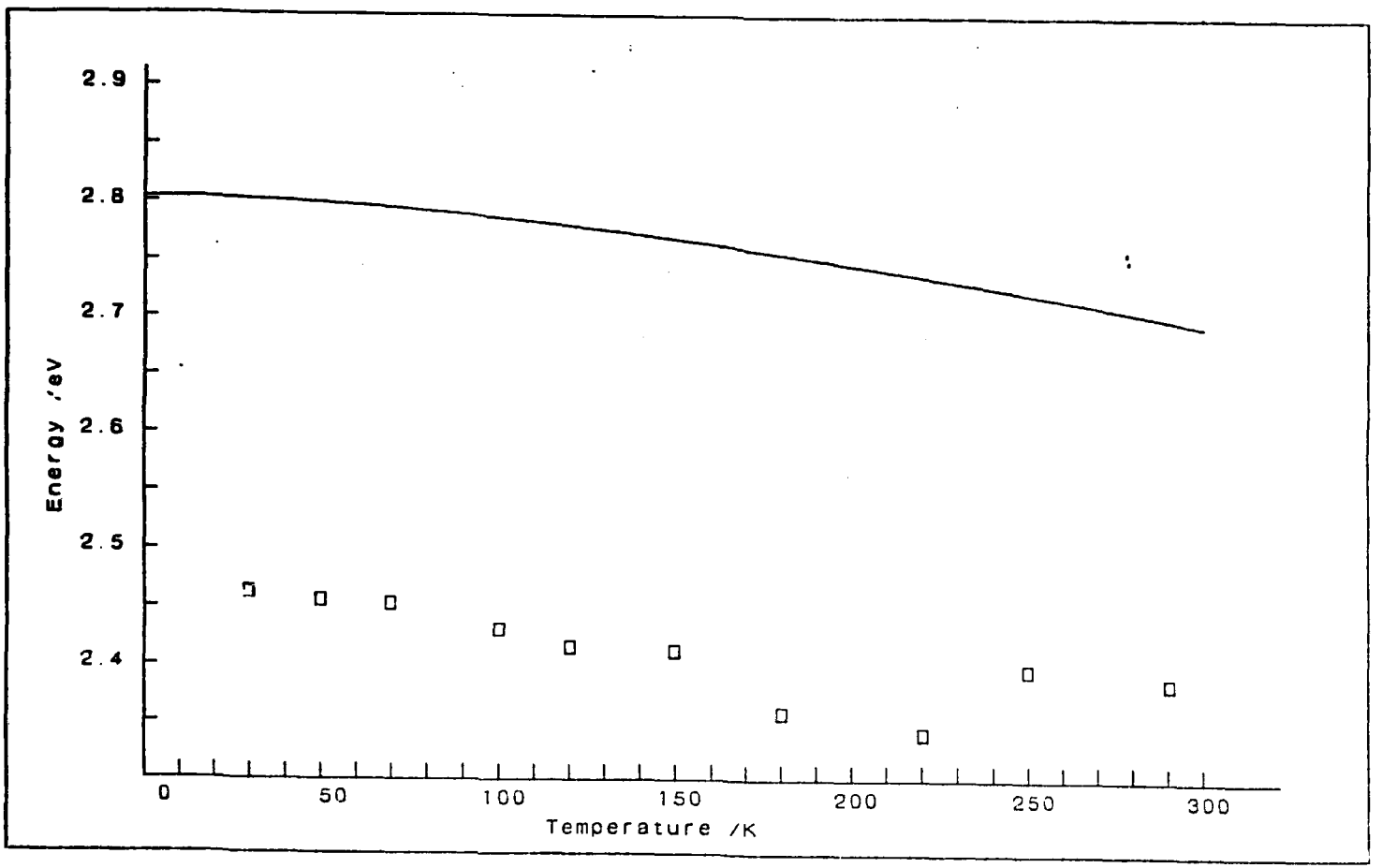
2.9
2.8
2.7
2.6
2.5
2.4
Energy /eV
0
50
100
150
200
250
300
Temperature /K

Fig. 18 ZnTe/InP